Hydrothermal processes at Gusev Crater: An evaluation of Paso Robles class soils

A. S. Yen,[1] R. V. Morris,[2] B. C. Clark,[3] R. Gellert,[4] A. T. Knudson,[5] S. Squyres,[6] D. W. Mittlefehldt,[2] D. W. Ming,[2] R. Arvidson,[7] T. McCoy,[8] M. Schmidt,[8] J. Hurowitz,[1] R. Li,[9] and J. R. Johnson[10]

Received 2 August 2007; revised 16 November 2007; accepted 18 December 2007; published 22 April 2008.

[1] The Mars Exploration Rover Spirit analyzed multiple occurrences of sulfur-rich, light-toned soils along its traverse within Gusev Crater. These hydrated deposits are not readily apparent in images of undisturbed soil but are present at shallow depths and were exposed by the actions of the rover wheels. Referred to as "Paso Robles" class soils, they are dominated by ferric iron sulfates, silica, and Mg-sulfates. Ca-sulfates, Ca-phosphates, and other minor phases are also indicated in certain specific samples. The chemical compositions are highly variable over both centimeter-scale distances and between the widely separated exposures, but they clearly reflect the elemental signatures of nearby rocks. The quantity of typical basaltic soil mixed into the light-toned materials prior to excavation by the rover wheels is minimal, suggesting negligible reworking of the deposits after their initial formation. The mineralogy, geochemistry, variability, association with local compositions, and geologic setting of the deposits suggest that Paso Robles class soils likely formed as hydrothermal and fumarolic condensates derived from magma degassing and/or oxidative alteration of crustal iron sulfide deposits. Their occurrence as unconsolidated, near-surface soils permits, though does not require, an age that is significantly younger than that of the surrounding rocks.

Citation: Yen, A. S., et al. (2008), Hydrothermal processes at Gusev Crater: An evaluation of Paso Robles class soils, *J. Geophys. Res.*, *113*, E06S10, doi:10.1029/2007JE002978.

1. Introduction

[2] The selection of Gusev Crater as a landing site for the Mars Exploration Rover Spirit was based on the goal of characterizing the nature and extent of aqueous processes at the Martian surface [*Golombek et al.*, 2003; *Cabrol et al.*, 2003]. The presence of Ma'adim Vallis, a 900 km valley debouching into the crater from the south, suggested that Gusev Crater was a location that might permit study of fluvial, lacustrine, and other aqueous processes. In addition, the proximity of Apollinaris Patera, an ancient volcano 250 km north of Gusev, suggested the possibility of magma-water interactions.

[3] After more than 150 sols on the Gusev plains where the geology was dominated by relatively unweathered olivine-rich basaltic soils and rocks, the first compelling evidence for significant water-related weathering at Gusev Crater was the discovery of goethite [*Morris et al.*, 2006], an iron oxyhydroxide, which requires the presence of water for its formation. In contrast to this finding, however, are numerous examples indicating that interactions with liquid water have been relatively minimal. For example, the discovery of an exposed ultramafic sequence of rocks [*Mittlefehldt et al.*, 2006] where over 70% of the iron is in unaltered olivine and the ferric to total iron ratio is only $\sim$0.1, comparable to unaltered shergottites [*Burns and Martinez*, 1991], indicates that certain materials within Gusev Crater have been minimally altered by aqueous processes. Even some of the most altered rocks in the Columbia Hills, such as the Watchtower Class rocks that dominate much of the northern side of Husband Hill, apparently underwent nearly isochemical alteration, suggesting very low water-to-rock ratios [*Ming et al.*, 2006; *Squyres et al.*, 2006].

[4] Analyses of several isolated occurrences of light-toned soil deposits excavated by the rover wheels provide additional compelling evidence of significant water-related activity at the Spirit landing site. These samples occur in

[1]Jet Propulsion Laboratory, California Institute of Technology, Pasadena, California, USA.
[2]NASA Johnson Space Center, Houston, Texas, USA.
[3]Lockheed Martin Corporation, Littleton, Colorado, USA.
[4]Department of Physics, University of Guelph, Guelph, Ontario, Canada.
[5]Department of Earth and Planetary Sciences, Arizona State University, Tempe, Arizona, USA.
[6]Department of Astronomy, Cornell University, Ithaca, New York, USA.
[7]Department of Earth and Planetary Sciences, Washington University, St. Louis, Missouri, USA.
[8]National Museum of Natural History, Smithsonian Institution, Washington, D.C., USA.
[9]Center for Mapping, Ohio State University, Columbus, Ohio, USA.
[10]U.S. Geological Survey, Flagstaff, Arizona, USA.

0148-0227/08/2007JE002978

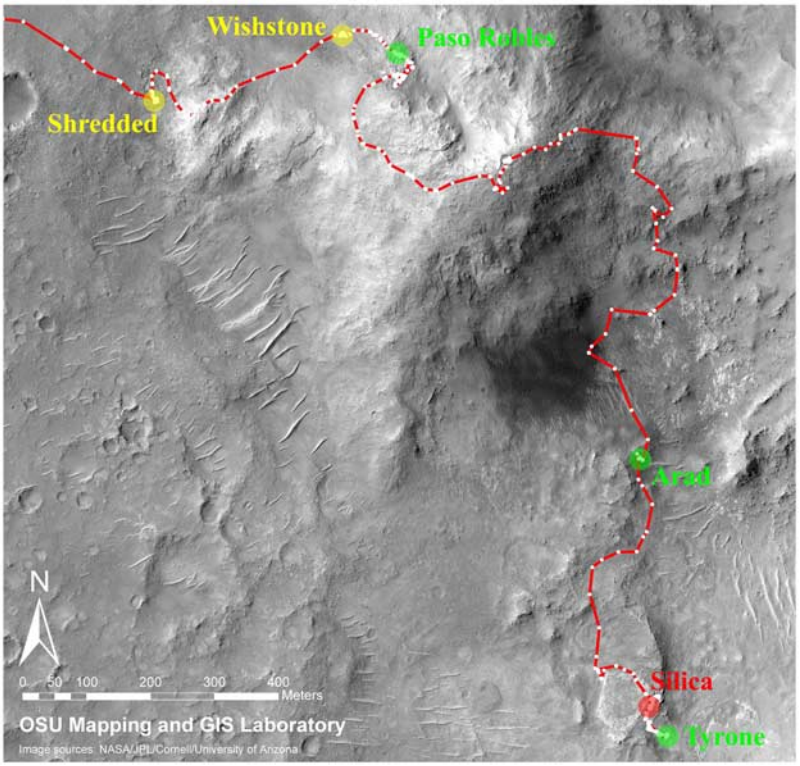

Figure 1. Locations of Paso Robles class soil exposures analyzed in detail by the rover instruments are shown in green superimposed on a High Resolution Imaging Science Experiment (HiRISE) image of the Husband Hill complex. The locations indicated in yellow represent the major suspected Paso Robles class soil exposures (not confirmed by the entire instrument complement). The location of the red circle indicates distinct, but likely related, deposits of amorphous silica. The red line illustrates the traverse of the rover.

two groupings: (1) The sulfur-rich Paso Robles class deposits, named after the first sample of such material that was analyzed by all of the rover instruments [*Gellert et al.*, 2006; *Morris et al.*, 2006; *Ming et al.*, 2006], and (2) the distinct, but related, silica-dominated materials encountered after sol 1150 (S. W. Squyres et al., Discovery of silica-rich deposits on Mars by the Spirit Rover, submitted to *Science*, 2008). There are a significant number of light-toned soils which were not analyzed by the in situ instruments, preventing classification into these two or possibly alternative groups. The focus of this work is the Paso Robles class soils, and a summary of the previously published and new sets of instrument data, reconstructions of possible mineralogies, candidate formation processes, and implications of these findings are discussed in sections 2–9.

2. Geologic Setting

[5] The Paso Robles class of light-toned soils encountered by Spirit is found on and around Husband Hill and within the Inner Basin (Figure 1). There are three confirmed locations with exposures of this soil class: The original "Paso Robles" site, "Arad" (also known as "Dead Sea"), and "Tyrone." (See R. E. Arvidson et al. (Overview of the Spirit Mars Exploration Rover mission to Gusev Crater, Columbia Hills: Independence outcrop to the ascent onto Home Plate, manuscript in preparation, 2008) for a description of the rover traverse.) Several additional occurrences of light-toned soil which may also be Paso Robles class deposits are indicated in Figure 1. The deposits at the Tyrone location are found in a shallow depression (Figures 2 and 3a) bounded primarily by the extensions of "Low" and "Mitcheltree" ridges to the west and the slopes of McCool Hill to the east. The Arad exposures occur at the base of a hill at the western margin of a ~150 m wide valley. There is an abrupt change in slope at this location, but unlike the Tyrone deposit, the Arad samples are not found within a defined topographic minimum (Figure 3b). Similarly, one of the possible exposures (not confirmed by in situ analyses) of Paso Robles class materials, referred to as "Shredded," also occurs near the base of a hillslope (Figure 3c). The location of the original Paso Robles measurements, however, does not appear to be influenced by topography and is on a slope of approximately 12° (Figure 3d). The suspected Paso Robles class materials near "Wishstone" (again, in situ analyses were not conducted) are also on comparable slopes (Figure 3e).

[6] The elevations of the Paso Robles class soils span a significant portion of the topographic range encountered by Spirit and do not exhibit a consistent pattern. For reference, the summit of Husband Hill is approximately 106 m above the elevation of the lander on the Gusev Plains. Exposures of Paso Robles class soils occur at approximately 33 m (Arad), 45 m (Tyrone), and 66 m (Paso Robles) above the lander elevation. The suspected, but not confirmed, expo-

Figure 2. Pancam false color view from the "McMurdo" panorama of the Tyrone deposit of Paso Robles class soils. The view is toward the east (facing McCool Hill). The exposed material (center) resides in a localized topographic depression. Material dragged from Tyrone by the rover wheels was deposited at the edge of the tracks.

sures of Paso Robles class soils at Shredded and Wishstone are found ~24 and ~45 m above the lander, respectively.

3. Instrument Analyses

[7] Paso Robles class deposits tend to be fine-grained and poorly compacted, which are soil properties that present challenges to rover mobility. In fact, several occurrences of light-toned soil, including Paso Robles itself, were first discovered when wheel slip impeded rover motion and excavated soil deposits around rover wheels. Microscopic Imager (MI) [*Herkenhoff et al.*, 2003] images (e.g., Figure 4) show weakly consolidated samples with clumps that may have been induced by mixing by the rover wheels. Pancam [*Bell et al.*, 2003] false color images of the major occurrences are shown in Figure 5. This visible/near-infrared data set exhibits relatively uncommon spectral features which are consistent with ferric sulfates with various levels of hydration [*Johnson et al.*, 2007]. Evidence that these deposits are hydrated is provided by a strong 6 μm molecular water feature observed in Mini-Thermal Emission Spectrometer (Mini-TES) [*Christensen et al.*, 2003] spectra (Figure 6). The focus of the work described here is on data collected from the Mössbauer [*Klingelhöfer et al.*, 2003] and Alpha Particle X-ray Spectrometers (APXS) [*Rieder et al.*, 2003].

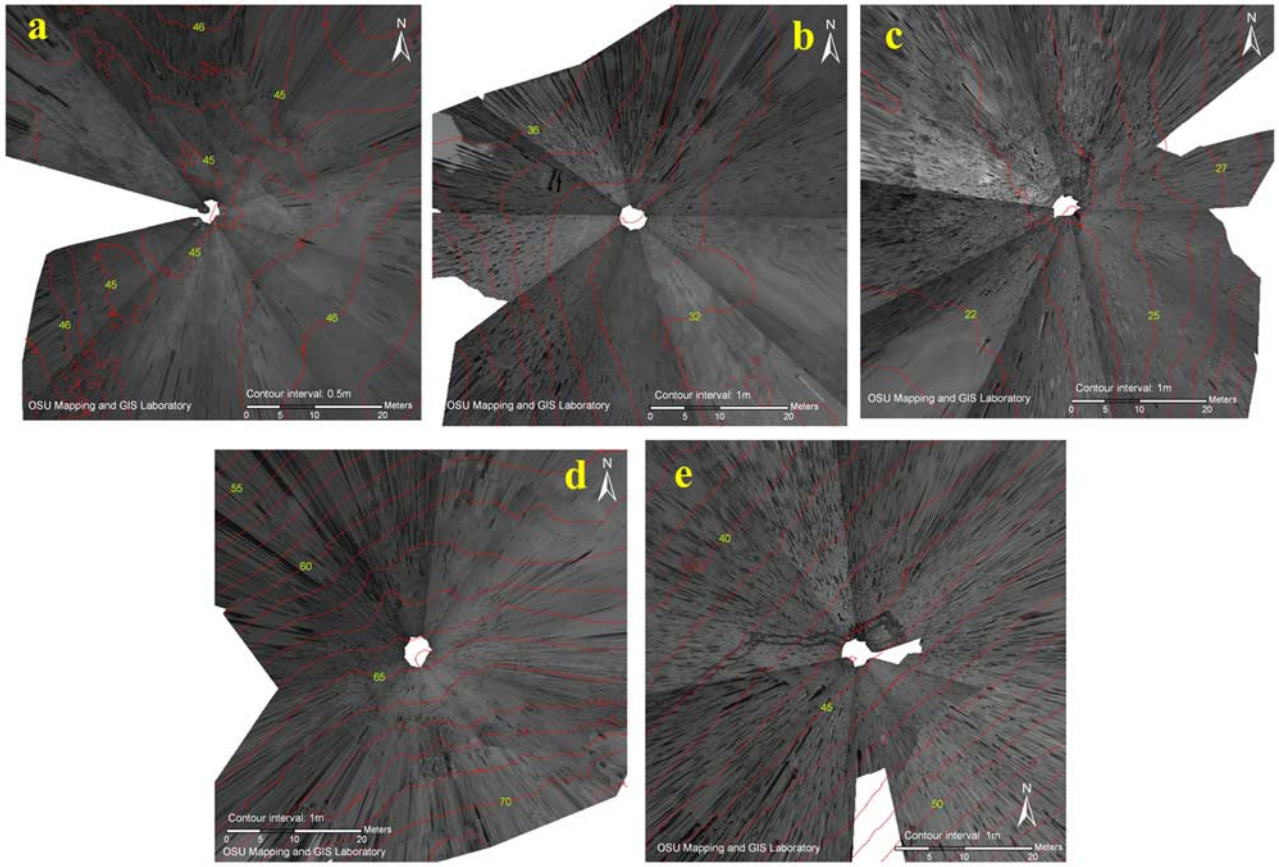

Figure 3. Paso Robles class soil deposits are found in a variety of situations relative to local topography (1 m topographic contours shown in red; white indicates areas not covered in the original images): (a) Tyrone in a localized depression, (b) Arad and (c) Shredded at the base of slopes, and (d) Paso Robles and (e) Wishstone on slopes of ~12°. Note that the Shredded and Wishstone exposures are not confirmed exposures of sulfur-rich soils.

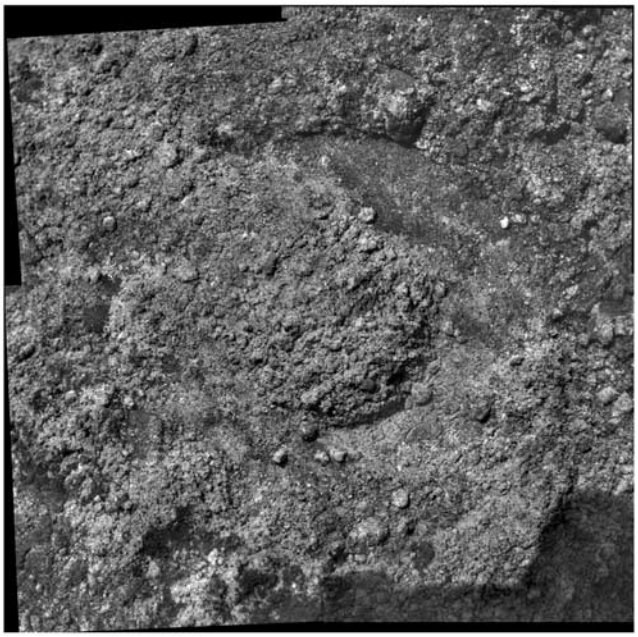

Figure 4. Mosaic of four Microscopic Imager images of light-toned soil at Paso Robles (sol 400, approximately 5 × 5 cm). The imprint of the Mössbauer contact sensor (37 mm outer diameter) is visible in the mosaic.

Table 1 lists the analyses conducted to date on this class of soil samples by these two instruments.

[8] The first in situ measurement of this class of soils was a short (~30 min) APXS analysis on a target called Pasadena Marengo at what is now referred to as the Paso Robles site. In this daytime measurement, elevated instrument temperatures significantly compromised the data quality but did not prevent the extraction of a signal that indicated a level of sulfur far greater than in any previous measurement at Gusev Crater. This exploratory measurement was followed by a longer, nighttime APXS analysis (Pasadena Paso Robles) at appropriate detector temperatures. An associated Mössbauer measurement of this sample was also obtained. After driving away from this location before the results could be fully assessed, the science team decided to return to the location for a more detailed evaluation, resulting in APXS and Mössbauer data from the Paso Robles2 PasoLight1 target. Measurements were also made in an attempt to extract the composition of the light-toned material from mixtures with typical Gusev (basaltic) soils. These two additional measurements (Table 1), however, were too close in composition to typical Gusev soils to be useful in mixing models. Thus, the Pasadena Paso Robles and the Paso Robles2 PasoLight1 analyses are the most useful of the data collected from this site for understanding the composition and origin of this class of soils. Interpretations of these data are given by *Morris et al.* [2006] and *Ming et al.* [2006]. In the text that follows, analyses at the Paso Robles "location" or "site" refers to these two measurements, and Paso Robles "class" soils refer to all exposures of light-toned soils at the Gusev site which have related compositions.

[9] The APXS and Mössbauer analyses of the light-toned soils at the Arad site (Samra and Hula) have not been previously published and provide additional insight into the formation of Paso Robles class soils. These samples are south of Husband Hill in the Inner Basin (Figure 1), and provide the measurements with the least contamination from surrounding basaltic soils. Each target was analyzed by the APXS, and Mössbauer data were collected from Samra.

[10] During the rush to find a north facing slope that would allow Spirit to survive its second winter on Mars, the rover became mired in the Tyrone deposit of light-toned soils, just southeast of Home Plate (Figure 1) (R. E. Arvidson et al., manuscript in preparation, 2008). A quick escape was necessary, and APXS and Mössbauer analyses were not conducted at that time. Studies of Tyrone were resumed the following spring. However, because of the possible risk of becoming permanently stuck at Tyrone, measurements were instead made on the material that had been fortuitously dragged out of the Tyrone area by the rover wheels and deposited on the edge of the wheel tracks (Berkner Island and Mount Darwin). The Berkner Island sample is approximately 40 m from the original Tyrone location while the Mount Darwin target is much closer at a distance of approximately 10 m.

3.1. Mössbauer Data

[11] Mössbauer spectra of Paso Robles class soils are dominated by narrow doublets indicative of ferric iron (Figure 7). The isomer shifts (δ), quadrupole splittings (ΔE_Q), and full widths at half maxima (Γ) of fits to the ferric doublets are listed in Table 2 (see *Morris et al.* [2006] for a description of these Mössbauer parameters). The dominant ferric doublet is assigned to Fe^{3+} sulfate [*Morris et al.*, 2006, 2007]. Variations in ΔE_Q and Γ, which are significantly greater than the 0.02 mm/sec uncertainties, may reflect ferric sulfates with different hydration states, different degrees of crystallinity, and/or different levels of substitutional impurities (e.g., Al^{3+} for Fe^{3+}). Because of the range of values of Γ and especially ΔE_Q, we attempted fits with two ferric doublets, but the quality of the fits did not improve significantly. Without a compelling reason to pursue more complex models, the results of the single doublet fits to the ferric signatures of Arad Samra and the two Paso Robles analyses are reported in Table 2. Other methods for fitting the data included the use of the ferric doublet parameters for Arad Samra as a constraint on the fits to the Paso Robles samples, but this approach did not produce reasonable results.

[12] The Tyrone Berkner Island and Mount Darwin samples had major contributions from typical basaltic soil, and the fidelity of the fits was enhanced by constraining the parameters of this soil component. The results of using the Mössbauer spectrum of the nearby Bear Island basaltic soil as a constraint on the fits to these two light-toned soils, as well as single doublet fits to the ferric signatures, are listed in Table 2. The use of other basaltic soil spectra in the constraints were also investigated, and the differences were within the uncertainty of the fits. The measurement at Tyrone Mount Darwin was further compromised by a larger than desired distance between the instrument sensor head and sample, resulting in poor counting statistics. In order to obtain area fractions of the iron minerals in Mount Darwin, it was necessary to constrain parameters of the ferric doublet using results from Tyrone Berkner Island measurement.

[13] Table 3 lists the percentage of total Fe associated with specific Fe-bearing phases as determined by the

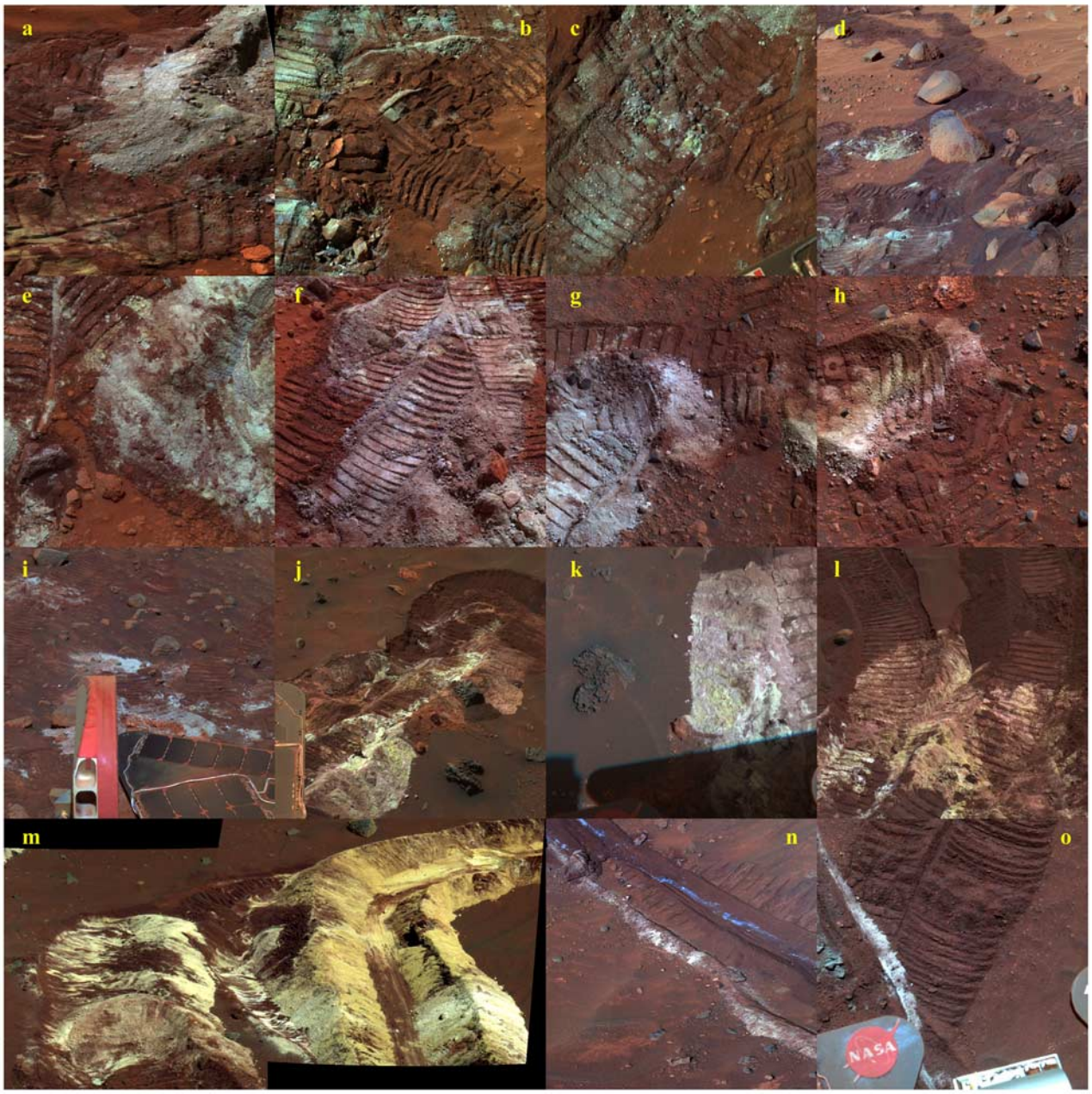

Figure 5. False color Pancam images of suspected (Shredded and Wishstone) and confirmed (all others listed) Paso Robles class soil exposures: (a–c) Shredded region (sol 180, p2387, p2544, p2545), (d) Wishstone area (sol 351, p2588), (e–f) PasoRobles1 (sol 400, p2551; sol 404, p2559), (g–h) PasoRobles2 (sol 431, p2599, p2530), (i) PasoRobles region (sol 445, p2548), (j–l) Arad area (sol 721, p2538, sol 723, p2542, sol 725, p2547), (m) Tyrone (sol 788, p2396), (n) Berkner Island (from "McMurdo Panorama"), (o) Mount Darwin (sol 1102, p2553).

Mössbauer spectrometer. The uncertainty is ±2% (absolute) for the Paso Robles and Arad measurements. The uncertainties in the Tyrone samples are higher because of larger quantities of basaltic soil and poor instrument positioning for the Mount Darwin analysis. The two measurements at Paso Robles, which are separated by a distance of only ~1 m, exhibit significant differences (over a factor of two) in the quantity of hematite. The measurement at the Arad location has the least amount of contamination from typical basaltic soils and one of the highest ferric to total iron ratios (0.91) measured to date by either rover.

3.2. Alpha Particle X-Ray Spectrometer Data

[14] The elemental compositions of Paso Robles class soil samples were determined by the APXS (Tables 4a and 4b). A defining attribute of these light-toned deposits is a sulfur content in excess of 30 wt % SO_3, unless the sample is significantly contaminated by typical Gusev basaltic soil

(Tables 4a and 4b). This elevated concentration of sulfur is the highest of all measurements made by either rover, including Meridiani outcrop rocks. The amounts of Na, Al, and K in Paso Robles class deposits are consistently lower than in typical Gusev soils and may represent minor levels of contamination from basaltic material. Calculations constraining the extent of basaltic soil mixing are described in section 4.

3.2.1. Compositional Variability

[15] Aside from elevated sulfur and variable contamination from basaltic soils, the collection of Paso Robles class materials does not display any clear or consistent chemical signatures. The two measurements of light-toned material at the Paso Robles site, which are separated horizontally by approximately 1 m, have differences in Al, P, Cl, K, Ti, Cr, Fe and Ni of 20% or greater. Similarly, the Samra and Hula samples at the Arad location are approximately 30 cm from each other and have greater than 30% differences in Na, Mg, Al, Si, Cl, Ca, Ti, Mn, and Zn. When comparing average measurements at Paso Robles with those at Arad, all measured elements with the exception of Fe and S are different in concentration by over 30%, with many differences exceeding 100%. Figures 8 and 9 illustrate the compositional variability of these analyses.

[16] The two measurements of material dragged from the Tyrone site are not substantially different from one another because they represent samples that were mixed within the rover wheel. The primary difference between the Berkner Island and the Mount Darwin analyses is a larger amount of basaltic soil in the sample (Berkner Island) that was dragged further from its origin. In comparison to the samples from the Paso Robles and Arad sites, the Tyrone material analyzed by the APXS contains approximately double the concentrations of Zn and Ca. It is clear that the chemical compositions of this class of soils are highly variable over both short and long distance scales. The variability in elemental composition precludes the possibility of extensive redistribution of materials from distant sources, which would tend to homogenize samples, and may be related to the observed color variations in these materials observed in Pancam data [*Johnson et al.*, 2007].

3.2.2. Localized Processes

[17] Chemical signatures of nearby rocks are evident in Paso Robles class soil deposits. For many elements, the compositions of the Paso Robles class soils are more similar to surrounding rocks than to other samples within this soil class (Figures 10 and 11). The most obvious indicator is the significantly elevated phosphorous at Paso Robles itself (4.7 and 5.6 wt % P_2O_5), where the nearby rocks are of Wishstone and Watchtower class. Members of this rock class have measured phosphate levels of up to 5.2% P_2O_5, the highest of all rocks found by either rover [*Ming et al.*, 2006; *Gellert et al.*, 2006]. A related indicator comes from a few tens of ppm yttrium, a trace element identified in Wishstone/Watchtower class rocks [*Clark et al.*, 2007], that is also present in the soil at the Paso Robles site (Figure 12).

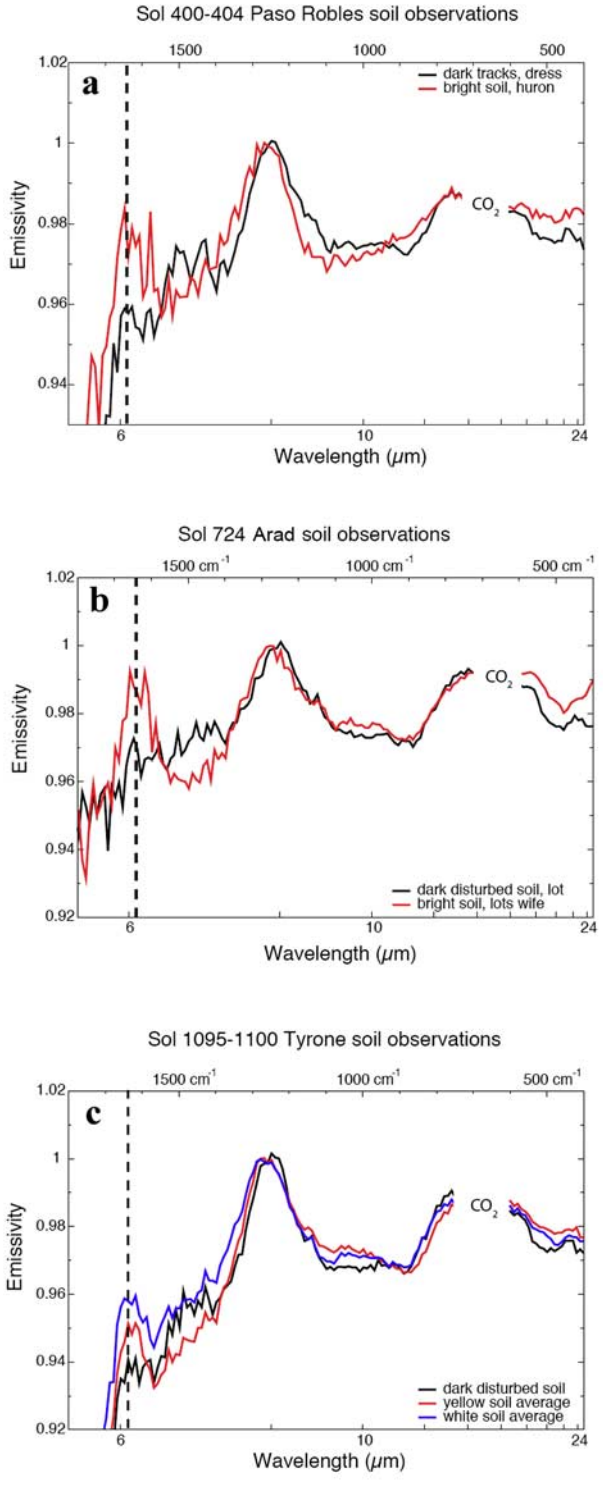

Figure 6. Mini-TES observations of Paso Robles class soils show enhanced hydration in a peak at 6 μm (dashed line in all plots). The light-toned soils are compared with dark disturbed soils in rover tracks at (a) Paso Robles (sols 400–404), (b) Arad (sols 721–724), and (c) Tyrone (sols 1095–1100). The exposures at Tyrone are the largest and include bright materials that are tinted yellow in addition to white [*Johnson et al.*, 2007]. Averages of the Mini-TES observations from each color unit are shown. In all areas the disturbed dark soil in rover tracks shows a small hydration peak due to the presence of dust [*Christensen et al.*, 2004] mixed with the basaltic sand in the soil. All spectra collected after sol 420 spectra have been corrected for dust accumulations on the mirror after the method described by A. T. Knudson et al. (manuscript in preparation, 2008).

Table 1. Summary of APXS and Mössbauer Spectrometer Data Collected from Paso Robles Class Soil Deposits

Sol(s)	Target	APXS	MB	Comments
399	Pasadena_Marengo	30 min	0	Warm detector. Indication of significant S
400–403	Pasadena_PasoRobles	3 h	47 h	First quality measurement of this material
426–428	PasoRobles2_PasoDark	6.5 h	6 h	Typical dark soil at Gusev
427–431	PasoRobles2_PasoLight1	6 h	27 h	
430	PasoRobles2_PasoDarkLight	9 h	0	Minor enhancements in P, S, Ti, Fe
723–726	Arad_Samra	13 h	33 h	Least amount of basaltic soil contamination
724	Arad_Hula	12 h	0	
1013–1016	Tyrone_BerknerIsland1	3 h	44 h	Deposit dragged from Tyrone by rover wheels
1098–1101	Tyrone_MountDarwin	3 h	22 h	Deposit dragged from Tyrone by rover wheels

Rare earth elements such as Y are largely held in phosphatic minerals such as whitlockite and apatite in Martian meteorites, and is therefore consistent with the elevated P. Another characteristic aspect of the rocks near Paso Robles reflected in the chemical analyses of nearby light-toned soils is anomalously low Cr (at detection limit) and Ni (~100 ppm).

[18] In contrast to the Paso Robles site, the soil measurements at Arad, which are on the south side of Husband Hill and not surrounded by phosphate-rich rocks, have only 0.5 wt % P_2O_5. Instead of showing similarities to Wishstone/Watchtower rocks, the Arad measurements appear to reflect the high Mg, Cr, and Ni and the low Al, K, Ca, and Zn of the Algonquin class rocks [*Squyres et al.*, 2007] exposed less than 150 m away. Yttrium is not observed in Arad soils.

[19] The Mount Darwin analysis of Tyrone materials contains the largest amount of CaO measured for Gusev samples (>9.0 wt %). This sample is diluted by ~40% contamination from basaltic soil (section 4.5), which averages ~6.3 wt % CaO, so the true Ca content of the Tyrone deposits could be in excess of 11 wt %. Within 40 m of the Tyrone exposure is the Halley Brunt sample, also with one of the highest CaO concentrations measured at Gusev (8.8 wt %). Unlike the previous examples of Paso Robles class deposits containing signatures of nearby rocks, the Halley Brunt target is not a primary igneous rock, and the possibility that these two materials formed via the same process cannot be ruled out. Nonetheless, taken collectively, it is clear that these light-toned soils are diverse in composition and chemically related to local rocks.

[20] Ratios of the measured elements in the Paso Robles class soils indicate that the chemical relationships to nearby rocks are not a result of physical admixtures of comminuted fines. The ratio of P to Ti in light-toned soils at the Paso Robles location, for example, is 4 to 5 times greater than in the surrounding rocks. In addition, the Samra measurement has the elevated Ni signature of local rocks, but no indications of the olivine which may be the host of the Ni. The chemical enrichments in the Paso Robles class soils which establish the connection to local rocks are in elements that are readily mobilized in aqueous solutions.

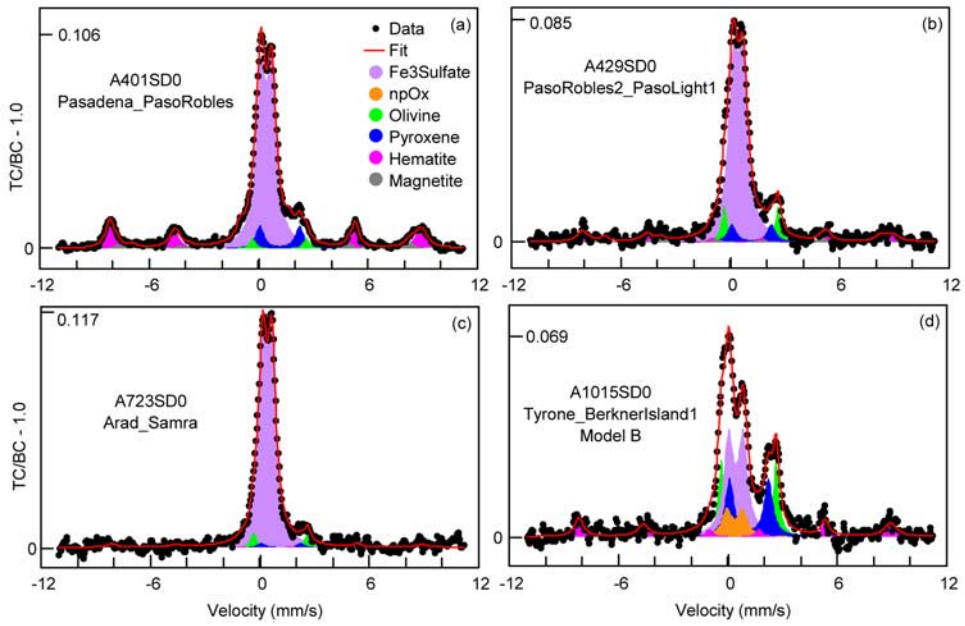

Figure 7. Mössbauer spectra for the S-rich, Paso Robles Class soils at Gusev crater. (a) Pasadena_PasoRobles; (b) PasoRobles2_PasoLight1; (c) Arad_Samra; and (d) Tyrone_BerknerIsland1 (model B, see Table 3). The spectrum for another S-rich soil (Tyrone MountDarwin) is similar to Figure 7d. Component subspectra for Fe in different Fe-bearing phases are shown by different colors, and the computed fit is shown by the solid red line. Values corresponding to TC/BC − 1.0 = 0 and its maximum value are shown on each *y* axis. TC, total counts; BC, baseline counts.

Table 2. Mössbauer Parameters δ, ΔE_Q, and Γ for the Fe3D2 (Fe^{3+}-Sulfate) Doublet Subspectrum[a]

	Generic Name (Assignment) Fe3D2 (Fe^{3+}-Sulfate)			
Target[b]	δ, mm/s	ΔE_Q, mm/s	Γ, mm/s	T, K
A401SD0 (Pasadena_PasoRobles)[c]	0.42[d]	0.62	0.60	190–280
A429SD0 (PasoRobles2_PasoLight1)[c]	0.43	0.55	0.68	200–280
A723SD0 (Arad_Samra)[e]	0.41	0.51	0.54	190–270
A1015SD0 (Tyrone_BerknerIsland1) model A[e,f]	0.42	0.81	0.63	190–250
A1015SD0 (Tyrone_BerknerIsland1) model B[e,g]	0.44	0.79	0.63	190–250
A1101SD0 (Tyrone_MountDarwin) model A[e,f]	[0.42][h]	0.78	0.57	190–270
A1101SD0 (Tyrone_MountDarwin) model B[e,g]	[0.44]	0.75	0.55	190–270

[a]MB parameters were calculated from spectra summed over the temperature interval given in the last column. Values of δ are with respect to metallic iron foil at the same temperature as the sample; δ is isomer shift; ΔE_Q is quadrupole splitting; Γ is full width.
[b]Target naming convention: AwwwwSD0 (Feature-name_Target-name); A = MER-A (Gusev Crater); wwww is Gusev Crater sol number that data product was returned to Earth; SD is disturbed soil. Alphanumeric strings before parentheses are unique target identifiers.
[c]Data from *Morris et al.* [2006].
[d]MB parameter uncertainty is ±0.02 mm/s.
[e]Data from *Morris et al.* [2007].
[f]From fit using one Fe^{3+} doublet.
[g]From fit using A1018SD0 (BearIsland_BearIsland) as the model for nonsulfate soil subspectrum.
[h]MB parameters in brackets are constraints used in the fitting procedure.

3.2.3. Hydration

[21] Scattering of the Pu X-ray lines emitted by the ^{244}Cm source of the APXS depends on the concentration of light elements that are not directly detected by the instrument, and this effect has been used to determine the extent of hydration in the Paso Robles class soils [*Campbell et al.*, 2008]. This approach is completely independent of the Mini-TES results shown in Figure 6, and produces results indicating 16 ± 8, 15 ± 6, 18 ± 5, 6^{+8}_{-5} wt % water for the analyses of Pasadena Paso Robles, Paso Robles2 Paso Light1, Arad Samra, and Arad Hula, respectively [*Campbell et al.*, 2008]. The specific mineralogical composition of the hydrated/hydroxylated phases, however, is not constrained by this analysis.

4. Mineral Mixtures

[22] The combination of the Mössbauer parameters for the narrow ferric doublet, the high Fe^{3+}/Fe_T ratio in the Mössbauer data, and the observation that Fe and S are the two most abundant elements after Si indicate that a primary constituent of Paso Robles class soils is ferric sulfate. Basaltic soil, other sulfates, and various nonsulfates are also present in these samples. Using a combination of APXS and Mössbauer data, sections 4.1–4.7 attempt to constrain the minerals phases.

4.1. Arad Samra

[23] The Samra sample at the Arad site is the most chemically pure example of Paso Robles class soils. The four most abundant of the measured elements expressed as oxides (SiO_2, SO_3, FeO, and MgO) constitute over 95 wt % of the material. Because of this relatively simple chemistry, calculating a candidate composition for Samra is more straightforward than for the other samples.

4.1.1. Basaltic Soil Contamination

[24] The Samra sample was originally covered with basaltic soil prior to excavation by the rover wheels. An

Table 3. Percentage of Total Fe Associated With Specific Fe-bearing Phases (f Factor Corrected) and Fe^{3+}/Fe_T (190–270 K) for Paso Robles Class Soils at Gusev Crater

	Generic Name[a]									
	Fe2D1	Fe2D2	Fe3D1	Fe3D2	Fe3D2	Fe3S1	Fe2.5S1	Fe3S2	Sum	Fe^{3+}/Fe_T
Phase Assignment[b] Target	Ol	Px	npOx	Fe3Sulfate	Mt	Mt(3)	Mt(2.5)	Hm		
A401SD0 (Pasadena_PasoRobles)[c]	3[d]	10	0	62	5	2	3	20	100[e]	0.86[f]
A429SD0 (PasoRobles2_PasoLight1)[c]	10	8	0	69	6	1	5	7	100	0.79
A723SD0 (Arad_Samra)[g]	7	3	0	86	0	0	0	4	100	0.90
A1015SD0 (Tyrone_BerknerIsland1) model A[g,h]	22	23	0	43	0	0	0	12	100	0.56
A1015SD0 (Tyrone_BerknerIsland1) model B[g,i]	22	23	[9][j]	34	0	0	0	12	100	0.56
A1101SD0 (Tyrone_MountDarwin) model A[g,h]	23	30	0	42	0	0	0	5	100	0.47
A1101SD0 (Tyrone_MountDarwin) model B[g,i]	22	31	[12][j]	30	0	0	0	5	100	0.47

[a]Names have the format FeXYZ: X is oxidation state of Fe, Y is D or S (doublet or sextet), Z is sequential number for subspectra having the same FeXY.
[b]Ol, olivine; Px, pyroxene; npOx, nanophase ferric oxide; Fe3Sulfate = Fe^{3+}-sulfate; Mt = magnetite; and Hm, hematite.
[c]Data are from *Morris et al.* [2006].
[d]Uncertainty in subspectral area is ±2% absolute unless stated otherwise.
[e]Because Mt = Mt(3) + Mt(2.5), Sum = Ol + Px + npOx + Fe3Sulfate + Mt + Hm. For all samples, ilmenite = 0.
[f]Fe^{3+}/Fe_T = (npOx + Fe3D2 + Mt(3) + 0.5(Mt(2.5)) + Hm)/Sum. Uncertainty in Fe^{3+}/Fe_T is ±0.03.
[g]Data are from *Morris et al.* [2007].
[h]From fit using one Fe^{3+} doublet. Uncertainty in subspectral area is ±4% absolute.
[i]From fit using A1018SD0 (BearIsland_BearIsland) as the non-sulfate soil spectrum with $A_{npOx} \sim 0.25(A_{Ol} + A_{Px})$ used as a constraint for the fitting procedure. Uncertainty in subspectral area is ±4% absolute.
[j]MB parameters in brackets are constraints used in the fitting procedure.

Table 4a. APXS Elemental Compositions Expressed as Weight Percent of Common Oxides[a]

Sol	Sample	Na_2O	MgO	Al_2O_3	SiO_2	P_2O_5	SO_3	Cl	K_2O	CaO	TiO_2	Cr_2O_3	MnO	FeO	Ni	Zn	Br
401	Pasadena_PasoRobles	1.64	5.53	4.13	21.8	5.61	31.7	0.55	0.19	6.84	0.62	0.04	0.25	21.0	109	98	494
427	PasoRobles2_PasoLight1	1.42	5.19	6.27	24.9	4.69	31.6	0.73	0.40	6.94	0.88	0.35	0.30	16.1	561	116	478
428	PasoRobles2_PasoDark	3.24	8.74	10.4	46.1	0.96	5.68	0.55	0.39	6.25	0.89	0.38	0.33	15.9	414	209	52
430	PasoRobles2_PasoDarkLight	3.02	8.64	9.72	43.2	1.38	7.73	0.58	0.38	6.39	0.99	0.37	0.34	17.2	395	235	69
723	Arad_Samra	0.14	4.04	1.21	37.7	0.50	35.1	0.31	0.01	0.81	0.53	0.48	0.05	19.1	748	67	92
724	Arad_Hula	0.39	11.5	2.46	28.4	0.51	32.8	0.66	0.04	5.15	0.25	0.46	0.13	17.2	887	91	72
1013	Tyrone_BerknerIsland1	1.98	7.09	6.21	36.9	0.88	22.1	0.39	0.28	7.62	0.50	0.43	0.25	15.2	747	191	82
1098	Tyrone_MountDarwin	1.06	6.54	5.06	32.9	0.95	27.6	0.42	0.27	9.02	0.51	0.51	0.18	14.8	781	246	86
-	Average Basaltic Soil[a]	3.07	8.62	10.3	46.5	0.87	5.76	0.68	0.43	6.31	0.88	0.34	0.33	15.9	464	271	43

[a]Ni, Zn, and Br are in ppm. Based on 20 high-quality measurements of fine-grained samples with no known irregularities.

upper limit on the amount of basaltic material mixed into the sample can be estimated by calculating how much of an average Gusev soil composition (Tables 4a and 4b) can fit within the Samra APXS measurement before any elemental concentrations are exceeded. Even without direct measurements of the chemical composition of the basaltic soil adjacent to Samra, this approach is appropriate given the compositional uniformity of typical Gusev soil [*Yen et al.*, 2005]. The amounts of Na and K in Samra are essentially at the detection limits. Accounting for the amount of these elements allowed by the measurement uncertainty results in a maximum of 5 wt % contamination from basaltic soil.

[25] Another approach for estimating the quantity of basaltic soil in Samra is using the Mössbauer results. Assuming that the olivine and pyroxene components of the Samra measurement originate from basaltic contamination, an average soil composition can be used to calculate the contribution from all measured elements. In this case, 10% of the iron is determined to be from the ferrous phases (Table 3). Scaling an average basaltic soil composition to match this iron content produces an estimate of 13 wt % for the amount of contamination from typical soils.

[26] A third technique involves extrapolation from a plot of Na versus Al for a variety of samples analyzed at Gusev Crater (Figure 13). Assuming that the roughly linear relationship represents a plagioclase feldspar component and that the only source of plagioclase in the measured material is from the basaltic soil, the upper limit for the basaltic soil component is approximately 3 wt %. This result is not independent of the limits based on Na and K calculated above, because Na is also used in this calculation. However, this approach does show that constraints using Al, in addition to Na and K, yield approximately consistent results.

[27] The difference between the 3% to 5% basaltic contamination calculated from APXS data and the 13% inferred from Mössbauer data may result from analysis area and depth differences. The APXS samples a ~30 mm diameter circular area to a depth of 2 to 100 μm, depending upon the energy of the X-ray [*Rieder et al.*, 2003]. The Mössbauer analyzes a 15 mm diameter circular region to a depth, depending on density, of 0.1 to 3 mm [*Klingelhöfer et al.*, 2003], more than an order of magnitude deeper than the APXS analysis. Lateral inhomogeneities may have resulted in more basaltic soil within the larger APXS field of view. Alternatively, the mixing of the dust and sand mantle by the rover wheels may have buried basaltic material under the immediate surface to a depth sampled by the Mössbauer spectrometer, but not by the APXS. The relative amounts of the two ferrous phases in Samra is not the ~1:1 ratio observed for typical basaltic soils, and the possibility that a small amount of an unidentified ferrous mineral phase contributes to the peaks assigned to olivine and/or pyroxene cannot be excluded. Given that the calculations described in this section for the Samra sample are based primarily on elemental chemistry, the 5% basaltic contamination derived from the APXS results is used.

[28] A significant implication of the relatively small amounts of basaltic contamination in the Samra deposit is that these light-toned materials have not been extensive redistributed from the location of initial formation. Fine grained basaltic sand and dust are pervasive in the Martian surface environment, and it is unlikely that the Paso Robles class materials could have been transported very far without developing a significant admixture of basaltic grains. The amount of typical Gusev soil that is observed in this deposit likely results from mixing of the surficial basaltic dust and sand layer by the rover wheels during the excavation process. These light-toned soils likely formed in the places they have been found.

4.1.2. Sulfates and Other Phases

[29] The Mössbauer analysis of Samra indicates that 4% of the iron (equivalent to 1% of the sample) is present as

Table 4b. Uncertainties in the APXS Values Listed in Table 4a

Sol	Target	Na_2O	MgO	Al_2O_3	SiO_2	P_2O_5	SO_3	Cl	K_2O	CaO	TiO_2	Cr_2O_3	MnO	FeO	Ni	Zn	Br
401	Pasadena_PasoRobles	0.21	0.09	0.07	0.24	0.14	0.30	0.02	0.06	0.06	0.07	0.03	0.01	0.12	49	18	26
427	PasoRobles2_PasoLight1	0.18	0.08	0.08	0.22	0.11	0.25	0.02	0.06	0.05	0.07	0.03	0.01	0.09	46	12	20
428	PasoRobles2_PasoDark	0.21	0.11	0.13	0.43	0.07	0.07	0.01	0.06	0.05	0.07	0.03	0.01	0.11	43	13	15
430	PasoRobles2_PasoDarkLight	0.26	0.12	0.11	0.40	0.08	0.08	0.01	0.06	0.05	0.07	0.03	0.01	0.11	40	12	15
723	Arad_Samra	0.14	0.06	0.03	0.26	0.07	0.24	0.01	0.05	0.01	0.06	0.03	0.00	0.07	41	8	14
724	Arad_Hula	0.16	0.12	0.04	0.26	0.07	0.27	0.01	0.05	0.04	0.06	0.03	0.01	0.10	44	9	16
1013	Tyrone_BerknerIsland1	0.28	0.13	0.11	0.40	0.09	0.24	0.01	0.06	0.07	0.07	0.04	0.01	0.12	55	16	17
1098	Tyrone_MountDarwin	0.28	0.15	0.11	0.33	0.10	0.30	0.02	0.06	0.09	0.07	0.05	0.02	0.10	78	28	21
-	Average Basaltic Soil[a]	0.20	0.10	0.11	0.40	0.07	0.08	0.01	0.06	0.04	0.06	0.03	0.01	0.10	39	12	15

[a]Values for average basaltic soil are for a typical individual measurement.

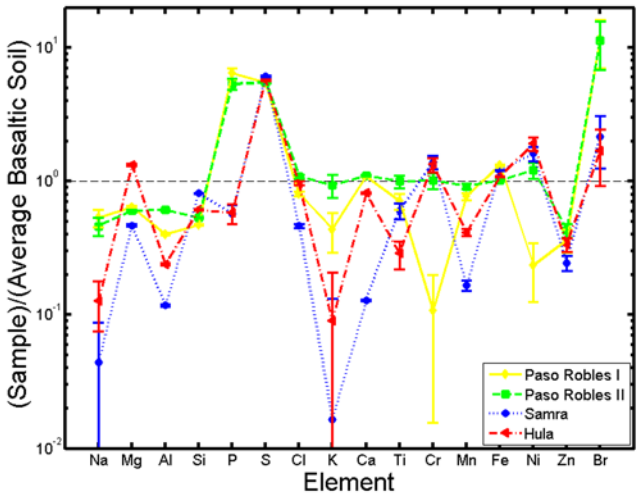

Figure 8. Elemental ratios of Paso Robles class soils to average Gusev basaltic soil (Table 4) illustrating significant differences from typical soils.

hematite. After removing the basaltic component and the hematite from the Samra analysis, the phases in which the remaining elements reside are not fully constrained. Candidate assemblages can be derived, but the results are not unique. The primary challenges include uncertainties in the total oxygen content, the absence of constraints on the abundance of $(OH)^-$ and H_2O groups, and not knowing if other undetected elements are abundant in the sample. Nonetheless, potential compositions can be reconstructed and examined for reasonableness.

[30] Calcium and phosphorous are minor components of the Samra deposit, and if they were combined into a Ca-phosphate, this phase would represent 1 wt % of the measured elements. The calculated Ca:P ratio is 1.3:1, but the uncertainty is sufficiently large that it could be as high as 1.7:1 as in the apatite family or as low as 1:1 as in brushite. At these low concentrations, Ca and P could

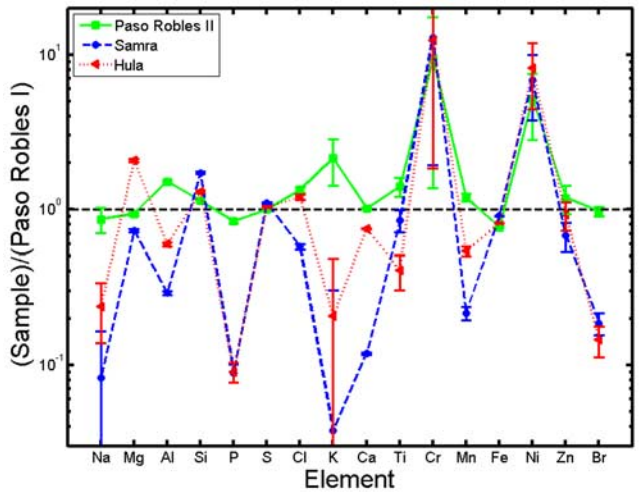

Figure 9. Elemental ratio plot of Paso Robles class soils to the first Paso Robles measurement indicating significant variability between the members of this soil class.

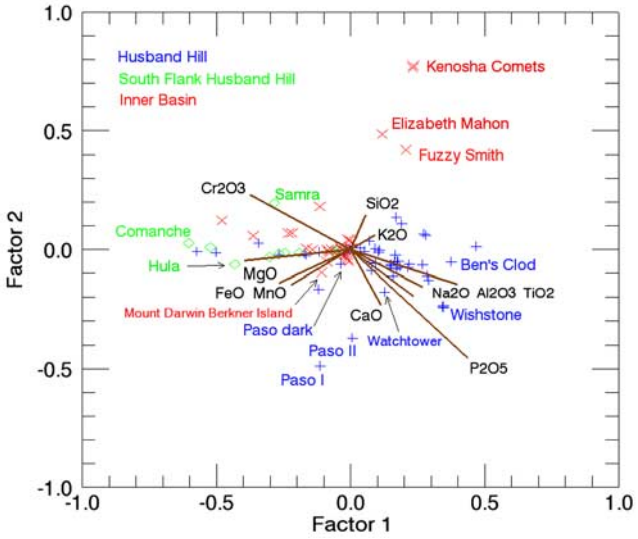

Figure 10. Correspondence analysis diagram [e.g., *Larsen et al.*, 2000] of samples analyzed by the Spirit APXS. The data points (colors) are grouped by geographic locations, and the brown lines represent the measured elements. Paso Robles class soils clearly plot within the field of nearby rocks.

also be substitutional impurities in other constituents without developing into a distinct mineral phase.

[31] Mg-sulfates have been detected in many locations at the Martian surface by the Mars Express OMEGA instru-

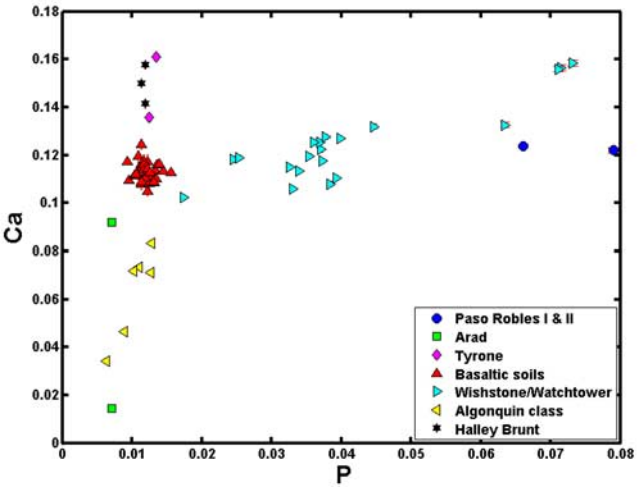

Figure 11. A molar Ca versus P plot indicating that signatures of nearby rocks are contained in the Paso Robles class soil measurements. The points representing the Paso Robles, Arad, and Tyrone deposits are widely separated indicating distinct compositions. However, soils at the Paso Robles site plot near Wishstone and Watchtower class rocks; Arad soils plot adjacent to Algonquin class rocks; and Tyrone soils are similar to Halley. Each of these rock types are found in reasonably close proximity to the associated Paso Robles class soil exposure indicating that for certain elements, these soils are more similar to nearby rocks than they are to each other.

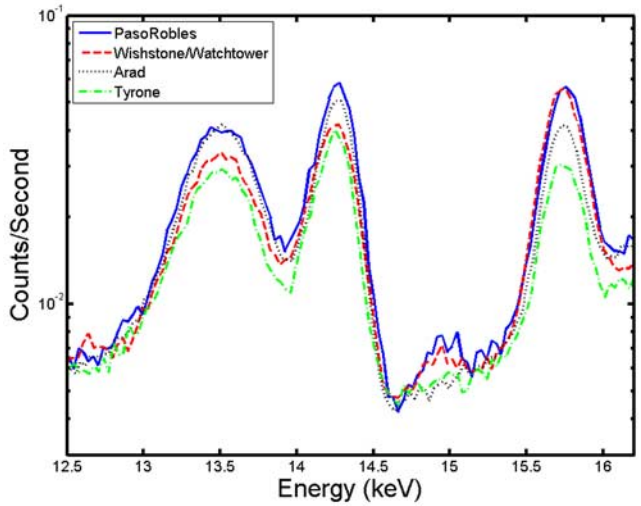

Figure 12. The trace element yttrium (peak at 14.9 keV) is found in the light-toned soil exposures at the Paso Robles location and in surrounding rocks. This element is not present in the Arad or Tyrone samples.

ment [*Bibring et al.*, 2005]. They are inferred to be present at Meridiani Planum on the basis of APXS data [*Clark et al.*, 2005], which is supported by Mini-TES [*Glotch et al.*, 2006] and orbital measurements [*Griffes et al.*, 2007]. It is therefore reasonable to consider the presence of an $MgSO_4 \cdot nH_2O$ phase in the Samra analysis. Assuming that all of the Mg is consumed in this phase with a Mg:S mole ratio of 1:1, 11 wt % of the sample would be present as a Mg-sulfate.

[32] The remaining Fe and S (46 wt %) can be combined at a Fe:S ratio of 2:2.8, which with uncertainties, fits well within the family of ferric sulfates of the form $(Fe^{3+})_2(SO_4)_3 \cdot nH_2O$ (see section 5.2 for additional discussion). After accounting for the phases listed above, the following remains: 34 wt % silica, 1 wt % Al (possibly substituting for the Fe^{3+} in the ferric sulfate), and 2 wt % Cl, Ti, and Cr. The possibility of excess silica in this analysis is inescapable, as there are few remaining elements for other compositions. In this reconstruction of candidate mineral phases, 90 wt % of Samra consists of silica, ferric sulfate, and Mg-sulfate. These compositions are summarized in Table 5. It is worth noting that such calculations assume end-member Fe-, Ca-, and Mg-sulfate mineralogy. It is possible that there could be some degree of solid solution among the various sulfate mineralogies [*Tosca and McLennan*, 2007].

4.2. Arad Hula

[33] The Hula sample at the Arad location appears similar in composition to Samra, but with nearly 3 times the Mg and over 6 times the Ca. Unfortunately, Mössbauer data were not collected from this sample because of the pressing need to move the rover to a safe location for the impending Martian winter, so direct information on the iron mineralogy is not available. The amount of basaltic soil contamination in this sample can be constrained to less than 15 wt % using Na and K as the limiting elements. This value is consistent with the 12% inferred from Figure 13, which is based on Na and Al in a plagioclase component.

[34] In order of abundance, the major remaining elements after the maximum amount of basaltic soil is subtracted are S, Si, Mg, Fe, and Ca. All other elements are present at approximately 3% combined. An attempt at charge balance using $(SO_4)^{2-}$, Mg^{2+}, Fe^{3+}, Ca^{2+}, and minor amounts of Al^{3+}, Cl^-, and $(PO_4)^{3-}$ indicates a significant excess (10 to 15 mole%) of cations. Si is assumed to be present as silica and not included in this attempted balance. This result suggests that oxides, hydroxides, oxyhydroxides, fluorides, borates and/or other silicates not present in the Samra sample are found in the Hula measurement just a few tens of centimeters away. Carbonates below approximately 10 wt % cannot be excluded on the basis of the alpha channel data [*Rieder et al.*, 2003] from the APXS, though it is unlikely that carbonates would form in combination with ferric sulfates. After removal of the basaltic soil and 21% silica, up to 57% of the remaining measured elements can be present as sulfates, with a maximum of 38%, 30%, and 9% of ferric sulfate (Fe:S = 2:3), Mg-sulfate (Mg:S = 1:1), and Ca-sulfate (Ca:S = 1:1), respectively.

[35] An alternative method for considering the composition of Hula is to calculate the limiting quantity of the Samra composition that can be accommodated by Hula. This maximum value is 56% with Si as the limiting element. In either approach to reconstructing the composition of Hula, it is clear that this sample is significantly different from the Samra deposit, that the difference does not result simply from admixture of basaltic soil, and that additional anions not directly measured by the APXS are necessary to maintain charge balance. The possible composition of Hula is summarized in Table 5.

4.3. Paso Robles I

[36] On the basis of the limited Cr abundance in APXS data, there can be a maximum of 15% basaltic soil in the first Paso Robles sample (Pasadena Paso Robles) that was analyzed in detail. The Mössbauer data, on the other hand, indicate that 3% of the iron is in olivine and 10% of the iron is in pyroxene, which corresponds to 28% basaltic soil when

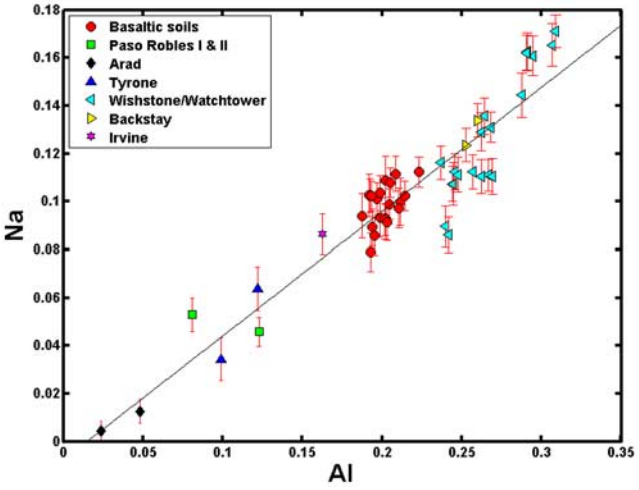

Figure 13. Molar plot of Na versus Al for rocks that are presumed to be plagioclase-rich and basaltic soils at the Gusev landing site. The fit to the plotted data approximately represents an An35 composition (andesine).

Table 5. Reconstructed Compositions of the Paso Robles Class Soils[a]

Sample	Basaltic Soil	Silica	Mg-Sulfate	Ca-Sulfate	Fe-Sulfate	Ca-P	Hematite	Other[b]
Arad_Samra	5	34	11	0	46	1	1	2
Arad_Hula	15	≤21	≤30	≤9	≤38	1	unknown	2
Pasadena_PasoRobles	20	12	11	0	37	11	5	4
PasoRobles2_PasoLight1	25	13	9	0	36	10	1	6
Tyrone_BerknerIsland1	65	6	4	8	14	1	1	1
Tyrone_MountDarwin	40	14	9	15	18	1	1	2

[a]Reconstructed compositions are in wt %.
[b]Represents percentages of measured elements that do not fit within the other columns of the table.

the contributions of the other elements are included. Calculations based on the possible inclusion of a plagioclase component (Figure 13) suggest up to 35% basaltic soil. Which of these values is likely to be the most representative? The estimate based on Na and Al is perhaps suspect in the Paso Robles samples given that the surrounding Wishstone and Watchtower class rocks have significant enhancements in these elements and because it is clear that these light-toned soil deposits reflect, to a significant degree, the chemistry of the local materials (section 3.2.2). That is, the Na and Al enhancements could, in this case, be unique attributes of the nonbasaltic portion of the Paso Robles sample, rather than a direct indicator of a basaltic soil contribution. This 35% value, however, is still valid as an upper limit for the basaltic contamination. The larger sampling depth and/or smaller field of view of the Mössbauer spectrometer relative to the APXS may be responsible for the larger amount of basaltic soil inferred from the Mössbauer measurement. There is also a possibility that an unidentified ferrous phase results in an overestimate of the amount of olivine and pyroxene, ultimately producing a larger estimate for the amount of basaltic soil. Accounting for possible uncertainties in the Cr measurement and the standard deviation in Cr values in over 35 Gusev soil measurements, both of which expand the limits of possible mixing, a value of 20% basaltic soil contamination was adopted for this reconstruction, but this value likely has an uncertainty of at least 5% absolute. Note that the low Cr signature of the nearby rocks [*Gellert et al.*, 2006] is not reflected in local basaltic soils, so establishing this constraint on the basis of Cr remains valid.

[37] After removal of 20% basaltic soil, 12% silica, and 5% hematite based on Mössbauer results, the primary remaining elements are S, Fe, Ca, Mg, and P in roughly a 15:8:4:4:3 molar ratio. Assuming these elements are present as $(SO_4)^{2-}$, Fe^{3+}, Ca^{2+}, Mg^{2+}, and $(PO_4)^{3-}$, overall charge balance is maintained to within a few percent. One possible composition of the sulfates and phosphates consistent with the APXS results is 37% $(Fe^{3+})_2(SO_4)_3 \cdot nH_2O$, 11% $MgSO_4 \cdot nH_2O$, and 11% $Ca_5(PO_4)_3(OH)$. See section 5.2 for additional discussion of the ferric sulfate phases. Evidence for significant amounts of Y in these samples is consistent with the presence of a distinct phosphate mineral. In shergottites, for example, the rare earth elements are dominantly contained in phosphates such as whitlockite and apatite [*McSween and Treiman*, 1998]. Other phases present in the first detailed Paso Robles analysis may include ~2% NaCl and ~3% Al as allophane [*Ming et al.*, 2006], alunite, or a substitutional impurity. This candidate composition for the first Paso Robles sample is summarized in Table 5. Other combinations of these elements are possible, but in all cases, ferric sulfates are still indicated. For example, the presence of ferric iron phosphates [*Lane et al.*, 2007] of up to 11% (e.g., $(Fe^{3+})(PO_4) \cdot nH_2O$ or $(Fe^{3+})_3(PO_4)_2(OH)_3 \cdot nH_2O$), cannot be excluded on the basis of elemental chemistry. If iron phosphates were present, a contribution from Ca-sulfates may be inferred. However, modeling of multispectral Pancam data of Paso Robles class soils did not detect any phosphates [*Johnson et al.*, 2007]. Mini-TES data of Paso Robles can be reasonably fit without ferric phosphates and the deconvolutions do not improve significantly when they are added (A. T. Knudson et al., Mini-TES derived mineralogy of soils at the Mars Exploration Rover "Spirit" landing site, manuscript in preparation, 2008). In addition, phosphates are a negligible component in two of the three major occurrences of this soil class (Table 4a) and are therefore not a defining characteristic.

4.4. Paso Robles II

[38] In the second set of analyses of the light-toned soils at the Paso Robles location (Paso Robles2 PasoLight1), the Mössbauer spectrometer places the tightest constraint on the amount of mixing from basaltic soil. Constraints based on Na with Al (Figure 13) and on Na alone both establish an upper limit of approximately 50% basaltic soil. With an estimated 10%, 8%, and 6% of the Fe reported by the Mössbauer analysis as olivine, pyroxene, and magnetite, respectively (Table 3), and perhaps a few percent of unreported nanophase ferric oxides obscured by the ferric sulfate doublet, up to 25% of the Fe could be present as a basaltic contaminant. Using analyses of average Gusev soils, this Mössbauer measurement corresponds to 30% of the observed Paso Robles II elemental composition. In previous examples (Samra and Paso Robles I), the Mössbauer results overestimate the quantity of basaltic material for reconstructions of the elemental chemistry. Therefore, a value of 25% basaltic soil is adopted for this analysis.

[39] After removal of 13% silica and 1% hematite, the remaining composition is roughly similar to the Paso Robles I analysis. The primary differences include ~20% less Mg and P, ~30% less Fe, and nearly double the amount of Al resulting in an Al abundance in Paso Robles II that is comparable to the quantity of Mg. While it is not necessary that all the Si be represented as silica, there is nearly as much Si as Al, Mg, and Ca combined, and the majority of these other cations are likely involved in sulfates and phosphates. Therefore, there is a significant likelihood that excess silica is present in this sample as well. Attempts at charge balance based on $(SO_4)^{2-}$, Fe^{3+}, Ca^{2+}, Mg^{2+}, and $(PO_4)^{3-}$ result in a 13% anion excess, but this can be remedied with the addition of Al^{3+}. One possible composi-

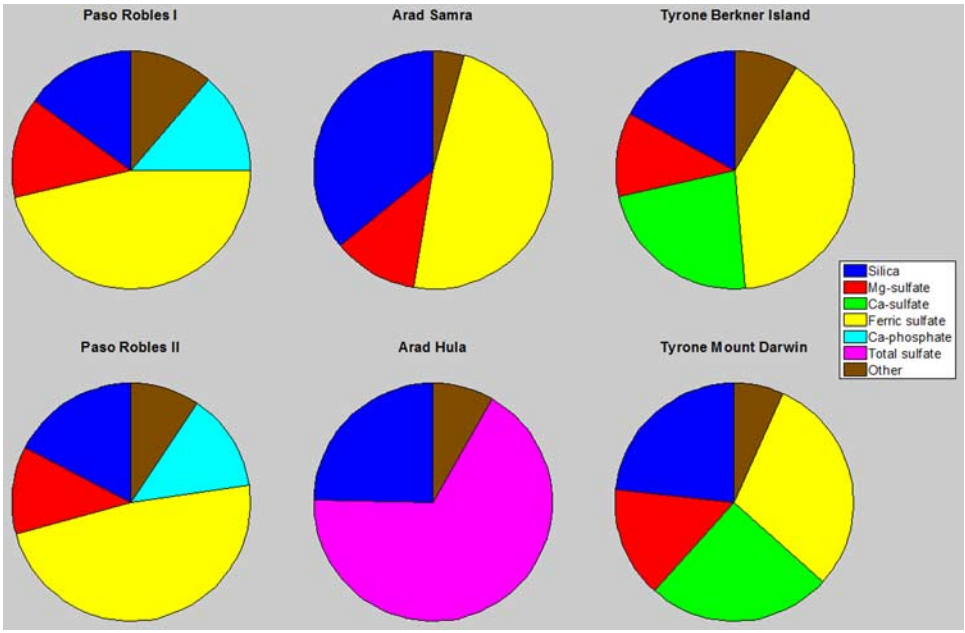

Figure 14. Derived compositions of the Paso Robles class samples after removal of basaltic soil contamination (based on Table 5). "Other" represents the remaining constituents after depicted phases and basaltic soil are removed. The available constraints on the Arad Hula sample prevent an accurate subdivision of the "total sulfate" wedge.

tion of the sulfates and phosphates consistent with the APXS results is 36% $(Al^{3+}, Fe^{3+})_2(SO_4)_3 \cdot nH_2O$, 9% $MgSO_4 \cdot nH_2O$, and 10% $Ca_5(PO_4)_3(OH)$. See section 5.2 for additional discussion of the ferric sulfate phases. Halite, at an abundance of up to 2%, may also be present. This candidate composition is summarized in Table 5.

4.5. Mount Darwin

[40] Light-toned soil dragged from Tyrone by the rover wheels created a thin trail that was mixed with and resting on top of basaltic soil (Figure 2). This material was accessible to the rover for analysis, and likely consists of a mix of the yellowish and the whiter components of the excavated soils (Figure 5m and *Johnson et al.* [2007]). The Mössbauer fits using an assumed abundance of npOx consistent with typical soil measurements suggest that approximately 60% of the iron is in components of basaltic soil. It should, however, be noted that the quality of the Mössbauer data from this target is extremely poor given a placement anomaly which resulted in a larger than desired standoff distance between the sensor head and the sample. When the Mössbauer results are scaled to account for all elements that are in average Gusev soils, the estimate for basaltic soil contamination is approximately 65%. However, given that the compositional analyses are based primarily on APXS data and because of the relatively poor quality of the Mössbauer data, we use instead the 40% upper limit for basaltic soil contribution established by APXS measurements of Na.

[41] A major difference between the Mount Darwin measurement and the analyses at Arad and Paso Robles is a significant abundance of Ca. Given that essentially all the P in this sample is from the basaltic soil contamination, the Ca is likely in the form of sulfates. Assuming Mg-sulfates (Mg:S = 1:1) and silica are in this sample, the major remaining component is the ferric sulfate with an apparent Fe:S of 1:1.1, which is well within the range expected for a plausible suite of phases (section 5.2). The candidate composition of Mount Darwin is summarized in Table 5.

4.6. Berkner Island

[42] The Tyrone Berkner Island1 sample is more distant from the original Tyrone deposit than Mount Darwin, and it is reasonable to expect it to be more diluted by basaltic soil. Five elements in the APXS analysis (Na, Al, Cl, K, and Ti) establish the allowable contribution of basaltic soil at approximately 65%, which is tighter than the constraints obtained from the Mössbauer results. After removing the basaltic contamination, candidate abundances of silica and Mg-, Ca-, and Fe-sulfates can be calculated as described in previous examples. The results are summarized in Table 5, and possible Fe-sulfate phases are discussed in section 5.2.

4.7. Mineralogical Summary

[43] The basaltic soil components estimated in the preceding paragraphs represent contaminants mixed in by the rover wheels and are not original constituents of the light-toned soil. It is therefore reasonable to remove the basaltic soil contribution and renormalize the remaining phases to determine the true composition of the Paso Robles class materials. The result (Figure 14) indicates that these deposits are dominated by silica, ferric sulfate, and Mg-sulfate. The measurements at the original Paso Robles location also contains phosphates, represented here as a Ca phase. The deposits excavated at Tyrone also contain significant Ca, likely present as a sulfate.

[44] In these renormalizations after basaltic soil removal, it is apparent that the Mount Darwin and Berkner Island samples are very similar in bulk chemistry, and hence in

Table 6. Candidate Ferric Sulfates in Paso Robles Class Soils[a]

Mineral Phase	Formula	Fe:S	1[b]	2[c]	3[d]	4[e]
Mikasaite	$(Fe^{3+})_2(SO4)_3$	2:3	X			
Lausenite	$(Fe^{3+})_2\ (SO_4)_3 \bullet 6H_2O$	2:3				
Kornelite	$(Fe^{3+})_2\ (SO_4)_3 \bullet 7-8H_2O$	2:3				
Coquimbite	$(Fe^{3+})_2\ (SO_4)_3 \bullet 9H_2O$	2:3	X			X
Paracoquimbite	$(Fe^{3+})_2\ (SO_4)_3 \bullet 9H_2O$	2:3	X			X
Quenstedtite	$(Fe^{3+})_2\ (SO_4)_3 \bullet 10-11H_2O$	2:3				
Butlerite	$Fe^{3+}(SO_4)(OH) \bullet 2H_2O$	1:1		X		
Parabutlerite	$Fe^{3+}(SO_4)(OH) \bullet 2H_2O$	1:1		X		
Fibroferrite	$Fe^{3+}(SO_4)(OH) \bullet 5H_2O$	1:1		X		X
Amarantite	$(Fe^{3+})_2\ O(SO_4)_2 \bullet 7H_2O$	1:1		X		
Hohmannite	$(Fe^{3+})_2\ O(SO_4)_2 \bullet 8H_2O$	1:1		X		
Metahohmannite	$(Fe^{3+})_2\ (SO_4)_2(OH)_2 \bullet 3H_2O$	1:1		X		
Ferricopiapite	$(Fe^{3+})_{2/3}(Fe^{3+})_4\ (SO_4)_6(OH)_2 \bullet 20H_2O$	7:9				X
Magnesiocopiapite	$Mg(Fe^{3+})_4\ (SO_4)_6(OH)_2 \bullet 20H_2O$	2:3				
Botryogen	$MgFe^{3+}(SO_4)_2(OH) \bullet 7H_2O$	1:2			X	
Hydronium jarosite	$(H_3O)(Fe^{3+})_3\ (SO_4)_2(OH)_6$	3:2	X			X
Rhomboclase	$H_5Fe^{3+}O_2(SO_4)_2 \bullet 2H_2O$	1:2			X	X
Schwertmannite	$(Fe^{3+})_{16}\ O_{16}(SO_4)_2(OH)_{12} \bullet nH_2O$	8:1	X			

[a]Ferrous phases are not listed as Mössbauer data constrain Fe^{2+} phases to less than 1% of the total.
[b]Not consistent with Mössbauer parameters.
[c]Fe:S of 1:1 implies ~5% excess sulfur at Arad Samra.
[d]Fe:S of 1:2 not compatible as the only ferric sulfate at Arad Samra.
[e]Identified as a possible constituent based on visible/near-infrared data [*Johnson et al.*, 2007].

inferred bulk mineralogy as well. This is as expected given that these analyses are from samples of the same material falling out of the rover wheels at different points along the traverse. The two Paso Robles samples are also similar to each other in bulk chemistry and inferred mineralogy but different from the Tyrone materials. The Samra deposit is unique because it does not contain a significant Ca phase. The Hula mineralogy remains the most poorly constrained of the six APXS analyses, because Mössbauer data were not acquired from this target and elements analyzed by APXS to not provide a satisfactory charge balance.

5. Acidic Environment

[45] Ferric sulfates form under oxidizing, low pH conditions [*Bigham and Nordstrom*, 2000], and it is therefore clear that these soils formed in a highly acidic environment. Furthermore, as discussed below, the possibility of elemental sulfur and/or unreacted sulfuric acid in Paso Robles class deposits cannot be excluded.

5.1. Excess Sulfur?

[46] A Fe:S ratio of approximately 2:3 is obtained directly from the reconstruction of the Arad Samra sample once the basaltic soil, measured hematite, silica, and Mg-sulfate (Mg:S = 1:1) are removed from elemental chemistry (section 4.1). This is a reasonably satisfying result given that $(Fe^{3+})_2(SO_4)_3 \cdot nH_2O$ is a common family of ferric sulfates (Table 6). This Fe:S ratio is also consistent with the chemical composition obtained from the other analyses of Paso Robles class soils. However, reconstructions of possible mineral phases based on elemental chemistry are not unique, even with good constraints on the iron oxidation states and certain identified iron-bearing minerals.

[47] Ferric sulfates in other forms cannot be excluded on the basis of the available data. Hydrogen in the deposit could be present as H_2O, $(OH)^-$, or both, and a dominant ferric sulfate in the Paso Robles samples of the form $(Fe^{3+})(SO_4)(OH) \cdot nH_2O$ is allowed by the APXS results. In this example, the Fe:S ratio is 1:1, implying approximately 6.5 mole% excess sulfur in the Samra analysis. Ferric sulfates with more Fe than S would result in even higher amounts of excess sulfur, which could be in the form of native S or possibly unreacted H_2SO_4. The available data do not require that excess sulfur be present, but they cannot exclude this possibility. In addition, it is also possible that native sulfur was a component of the original deposit and was subsequently oxidized to sulfate phases.

5.2. Ferric Sulfate Phase(s)

[48] The specific mineral form(s) of the iron sulfate(s) present in Paso Robles class soils can be constrained using the available instrument data. Possible phases are listed in Table 6. Only ferric phases are listed because minerals dominated by ferrous iron are not consistent with the Mössbauer results and cannot be significant contributors to the overall composition. Models using Pancam visible/near-infrared data indicate that rhomboclase, fibroferrite, hydronium jarosite, and/or ferricopiapite could be significant contributors to Paso Robles class soils [*Johnson et al.*, 2007]. The likelihood of the various candidates in Table 6 as dominant ferric sulfates in Paso Robles class soils can also be evaluated on the basis of iron-sulfur ratios. Phases with Fe:S of 1:1.5 fit well with APXS measurements of all Paso Robles class deposits. Lower ratios (e.g., Fe:S of 1:1) would imply excess sulfur (section 5.1) or a large contribution from unmeasured cations such as H^+, H_3O^+, or NH_4^+, though NH_4^+ is unlikely given the oxidizing conditions implied by the presence of ferric phases. Higher ratios (e.g., Fe:S of 1:2) can be present in low concentrations, but cannot be supported as the primary phase in the Samra analysis. Even if all of the Mg were in nonsulfates, the maximum Fe:S would be 1:1.8 in Samra. The percentage of Fe in the sulfate is well constrained by the Mössbauer spectrometer, and the measured abundance of S is insufficient to achieve a ratio of 1:2. This result excludes phases such as rhomboclase as the only ferric sulfate in Samra, though mixtures with other phases to reduce the average Fe:S ratio are allowed.

Multiple phases present as solid solutions may also be possible.

[49] The Mössbauer parameters of the ferric sulfate listed in Table 2 can be used to specifically exclude certain phases. Mikasaite [*Nomura et al.*, 2005], coquimbite and paracoquimbite (R. V. Morris, unpublished laboratory data, 2007), for example, exhibit quadrupole splittings (ΔE_Q) which are too narrow to be consistent with the Paso Robles class soils. Jarosite [*Klingelhöfer et al.*, 2004; *Morris et al.*, 2007], the nanophase ferric oxide (npOx) [*Morris et al.*, 2004, 2006] identified in other Martian samples, and schwertmannite, which is similar to np-Ox in Mössbauer analyses, all have distinctly different parameters from the Paso Robles class measurements. Identifying or excluding other phases listed in Table 6 on the basis of laboratory measurements are complicated by the metastability of many of these hydrated phases and the corresponding challenges associated with verifying the true mineralogical composition of the material analyzed.

[50] Establishing the mineral phases present in the Paso Robles class soil deposits is clearly important for determining the nature of the formation environment. However, many of the phases listed in Table 6 which are not specifically excluded by the Mössbauer data form in close association with each other in a well-defined environment. For example, on Earth, lausenite, kornelite, quenstedtite, butlerite, parabutlerite, fibroferrite, amanterite, hohmannite, metahohmannite, ferricopiapite, magnesiocopiapite, botryogen, and rhomboclase generally form together as precipitates of oxidative weathering of iron sulfide deposits [*Jambor et al.*, 2000; *Bigham and Nordstrom*, 2000]. Thus, identifying the presence of ferric sulfates in general, may provide nearly as much information about the formation environment of Paso Robles class soils as establishing the relative proportions of the specific phases themselves.

6. High-Temperature Environment

[51] The Home Plate feature within the Inner Basin is likely an accumulation of pyroclastic materials resulting from explosive interactions between basaltic magma and water [*Squyres et al.*, 2007]. All of the confirmed exposures of Paso Robles class soils are within 1 km of Home Plate, and Tyrone is only 50 m from the margin of the feature. Few constraints for establishing the relative ages of Home Plate and Paso Robles class soils are available, but it is clear that both water and high temperatures were available in the vicinity of Paso Robles class soil exposures at some point in Martian history.

[52] Geochemical evidence is also consistent with formation of Paso Robles class soils at elevated temperatures. The reconstructions of elemental chemistry described in section 4 indicate the presence of silica in Paso Robles class soils. After removal of the basaltic soil component, the concentrations of Na, Mg, Al, K, and Ca are relatively low. In the Samra analysis, for example, the molar abundance of Si is five times greater than the amount of these other five elements combined. With at least some of the Mg and Ca in sulfates and/or phosphates, there are not enough cations for typical silicate mineral phases. Thus, the occurrence of excess silica in these soils is indicated. There are at least two possible mechanisms for developing these silica deposits: (1) precipitation from solutions rich in dissolved silica and (2) acid bleaching of preexisting silicate phases. Both of these processes are suggestive of interactions with fluids and/or gases at elevated temperatures.

[53] The solubility of silica is relatively independent of pH under acid to neutral conditions [*Alexander et al.*, 1954; *Krauskopf*, 1956] but strongly dependent on the temperature of the fluid [*White et al.*, 1956]. This relationship is commonly used as a geothermometer in hydrothermal systems [*Fournier and Potter*, 1982]. Water in aquifers heated geothermally interacts with subsurface rocks liberating silica and other species in both acid sulfate and neutral chloride environments. As silica-saturated solutions rise to the surface and cool, precipitates of excess silica are formed. This process occurs at Yellowstone National Park where the interactions between thermal waters and volcanic rocks maintain up to 750 ppm silica in solution prior to cooling, evaporation, and precipitation of amorphous silica [*Channing and Butler*, 2007]. Elevated temperatures are consistent with the development of silica in Paso Robles class soils, but are not required. In the absence of hydrothermal and biological activity, 120 ppm silica could still be present in aqueous solution. Low-temperature, evaporitic sediments at Meridiani [*McLennan et al.*, 2005], for example, contain approximately 25% silica [*Glotch and Bandfield*, 2006].

[54] An alternative mechanism for concentrating silica is through acid bleaching, which, in contrast, likely requires elevated temperatures. In this process, dissolution of rocks and soils by acidic fluids and vapors (e.g., sulfuric and/or hydrochloric) is followed by immediate reprecipitation of amorphous $SiO_2 \cdot nH_2O$ and typically anatase (TiO_2 polymorph) [*Morris et al.*, 2000]. Other elements are leached resulting in high concentrations of silica with elevated Ti. A likely example of this process is found in the Kenosha Comets sample at the eastern margin of Home Plate. This light-toned soil contains over 90 wt % silica and 50% more Ti than average basaltic soil. A number of high-silica, light-toned soils distinct from the high-sulfur Paso Robles class materials have been analyzed near Home Plate. The Si to Ti ratios of the high-silica and the Paso Robles class materials are comparable, suggesting that these soils are related. The proximity of the Kenosha Comets sample to Tyrone ($\sim$50 m away) also supports a coupled relationship. Formation at elevated temperatures is likely for both classes of light-toned soils.

7. Formation Mechanism

[55] What processes resulted in the deposition of Paso Robles class soils? How did the material form initially, and what, if any, mechanisms may have redistributed or otherwise altered the deposits?

[56] The attributes of these deposits discussed in sections 2–6 will help address these questions. Paso Robles class soils (1) contain chemical signatures of local rocks, (2) display significant compositional heterogeneity over distances of tens of centimeters, (3) exhibit major differences in composition across the analyzed exposures, (4) contain mineral phases indicative of formation in an acidic environment, (5) are hydrated, (6) contain indicators consistent with high-temperature processes, (7) are found in a variety of geologic settings relative to topography and elevation,

and (8) have not been extensively redistributed and likely formed in the places where they were discovered.

[57] It is clear from this evidence that water played a key role in the formation of these deposits. A number of possible scenarios involving aqueous processes are presented in the following paragraphs.

7.1. Scenario 1: Lacustrine Sediments

[58] Paso Robles class soils precipitated from low-temperature aqueous solutions in local lacustrine settings. The occurrence of the Tyrone deposit in a localized topographic depression (section 2) led to the suggestion that it might have formed as layered aqueous precipitates from standing bodies of water [*Wang et al.*, 2007]. Other light-toned soils rich in ferric sulfates, however, are found on slopes of approximately 12° (section 2), indicating that topographic control in the formation is not important. Assuming a consistent process for the development of all Paso Robles class materials, the observed distribution argues strongly against the idea that these soils are precipitates from standing water. In addition, highly variable compositions over lateral distances of less than 1 m contradict the possibility of a quasi-equilibrium aqueous precipitate resulting from the evaporation of water. We therefore conclude that the origin of Paso Robles class soils as a lacustrine sediment is unlikely.

7.2. Scenario 2: Seeps and Efflorescent Salts

[59] Water interacting with subsurface iron sulfides migrated toward the surface (e.g., by capillary action) and rapidly evaporated resulting in a nonequilibrium accumulation of mineral precipitates. Water interacting with iron sulfides in the terrestrial environment can produce low pH solutions that precipitate minerals such as gypsum, copiapite, alunogen, metahohmannite, coquimbite, and paracoquimbite [*Joeckel et al.*, 2005]. Rhomboclase, ferricopiapite, bilinite, gypsum, hexahydrite, and Al-sulfates are commonly produced in acid mine drainages [*Keith et al.*, 2001; *Nordstrom and Alpers*, 1999]. Many of these phases are consistent with the possible mineralogies of the Paso Robles class soils and are stable in an arid environment. Thus, the observed mineral assemblages in Paso Robles class soils may be reasonable for an evaporitic deposit resulting from fluid interactions with local rocks. The substantial heterogeneities over short length scales imply low water-to-rock ratios, and the occurrence on slopes implies rapid evaporation upon exposure to the atmosphere.

[60] Several observations, however, present challenges to this formation scenario. The Paso Robles exposure of light-toned soil occurs approximately 66 m above the Gusev plains and 40 m below the summit of Husband Hill. Low-temperature seeps and fluid drainage would not be expected at this elevation; thermally driven processes may be more likely. In addition, efflorescent salts are typically found as cements in preexisting sediments [*Joeckel et al.*, 2005] rather than as widespread deposits of high purity. Furthermore, evidence that Home Plate is a hydrovolcanic deposit and the formation of, likely related, silica-rich deposits by acid sulfate bleaching processes indicate that thermal processes have been important in at least the Inner Basin. With the available observations, the development of Paso Robles class soil deposits through low-temperature seeps and evaporative processes cannot be ruled out, but a hydrothermal scenario seems more plausible.

7.3. Scenario 3: Phreatic Eruption

[61] Volcanic eruptions into near-surface water produced steam explosions which distributed ash layers to the observed locations of the Paso Robles class soils. The Home Plate feature has been interpreted as a construct of explosive volcanism [*Squyres et al.*, 2007], so it is reasonable to consider the possibility that Paso Robles class soils formed hydrothermally during magma interactions with water. Although mineral phases such as cristobalite, tridymite, and gypsum can form in such events, magmatic mineral phases generally dominate the deposits [*Ohba and Nakagawa*, 2002]. In addition, the observations of significant compositional diversity over both large and small length scales are not consistent with an air fall deposit. Settling from the atmosphere would tend to produce deposits that were more uniform in composition over a large area. Instead, the signatures of local rocks in these soils are strong indicators that the formation process operates on local rather than regional scales. It is also not clear how concentrations of ferric sulfates and silica could form in abundance under these conditions. A phreatic eruption scenario is therefore unlikely to be responsible for the formation of Paso Robles class soils.

7.4. Scenario 4: Fumarolic and Hydrothermal Deposits

[62] Paso Robles class soils formed as condensates of gas emissions and precipitates from hydrothermal fluids associated with nearby volcanic processes. The Home Plate structure is likely a remnant of an explosive volcanic deposit [*Squyres et al.*, 2007], indicating that heated volcanic fluids and gases were once common in this vicinity. Significant involvement of volatiles in the Home Plate region is also evidenced by the abundance of alkali-rich vesicular basalts [*Crumpler et al.*, 2007]. Abundant volatiles in a volcanic setting are clearly consistent with the likelihood of fumarolic emissions and hydrothermal precipitates.

[63] Of the likely mineral phases identified in Paso Robles class soils, silica, gypsum, anhydrite, and hematite are commonly found in fumarolic deposits on Earth [*Africano and Bernard*, 2000; *Keith*, 1991]. Ferric sulfates in terrestrial occurrences are typically associated with acid mine drainages, but there is clear evidence for copiapite, quenstedtite, fibroferrite, coquimbite, and other Fe hydroxysulfates as fumarolic condensates [*Zimbelman et al.*, 2005; *Stoiber and Rose*, 1974]. The occurrence of ferric sulfates is supported by thermochemical modeling of products formed by rapid cooling of volcanic gases which predicts the formation of $Fe_2(SO_4)_3 \cdot H_2O$ [*Getahun et al.*, 1996]. In addition, kieserite, hexahydrite, and epsomite have been reported [*Stoiber and Rose*, 1974]. The relative simplicity of the likely mineral assemblages in the Paso Robles class deposits is not unprecedented. Examples of fumarolic sublimates consisting of sulfur, gypsum, halotrichite, and little else have been reported [*Stoiber and Rose*, 1974]. Furthermore, it is possible that an initially complex assortment of metastable phases equilibrated with the ambient environment over geological timescales producing the observed compositions. Thus, the likely mineral phases in Paso Robles class deposits are consistent with fumarolic deposits.

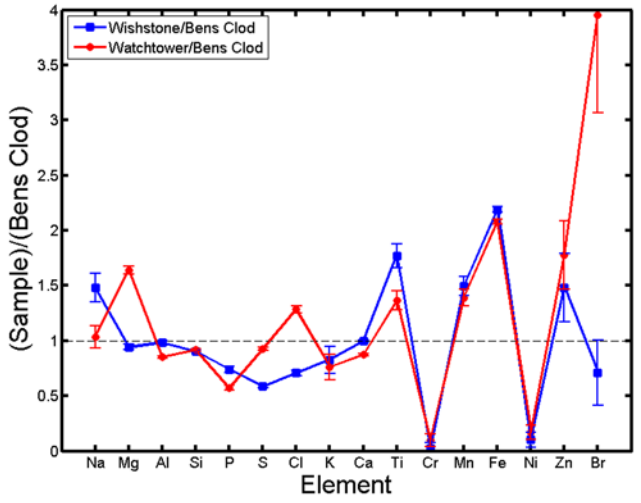

Figure 15. Ratio of Wishstone average (blue) and Watchtower average (red) compositions to the composition of Ben's Clod, a small Ti- and P-rich rock found at the Paso Robles location. The precursor to Ben's Clod may have been of the Wishstone/Watchtower class.

[64] Zinc and potassium are elements characteristically enhanced in high-temperature regions of terrestrial volcanic sublimates [*Symonds et al.*, 1987] which are also detectable by the Mars Exploration Rover (MER) APXS. The highest concentrations of Zn and K thus far detected on Mars are within a few tens of meters of the Tyrone exposure of Paso Robles class soils. The sample with the highest Zn levels (nearly 2300 ppm) contains hematite and exhibits compelling evidence for Ca-sulfate [*Yen*, 2006], both of which are common fumarolic minerals. Neither Zn nor K concentrations are significantly enhanced in the Paso Robles class soils themselves, which may indicate that they are more distal deposits or formed from fluid runoff of vapor condensates.

[65] The chemical signatures of the local rocks in analyses of the Paso Robles class soils is indicative of fluids and vapor migrating through subsurface materials prior to forming precipitates at the surface. Heterogeneities in the composition over short length scales are characteristic of fumarolic deposits, which are nonequilibrium condensates. The occurrence of hematite and, particularly, silica are consistent with formation in a high-temperature environment. The apparent fractionation of S-rich vapors (producing the Paso Robles class soils) and Cl-rich brines (indicated in analyses of rocks at Home Plate [*Squyres et al.*, 2007]) may be related to boiling of a hydrothermal brine at depth (M. Schmidt et al., The hydrothermal origin of excess halogens at Home Plate, Gusev Crater, submitted to *Journal of Geophysical Research*, 2007).

[66] Bleaching by acidic volatiles (e.g., fumarolic gases and vapor condensates) is indicated by several high-silica analyses near Home Plate (section 6 and Squyres et al. (submitted manuscript, 2008)). In addition, a rock sample ("Ben's Clod") found at the Paso Robles location may represent a precursor to the smectite montmorillonite or its chemical equivalent [*Clark et al.*, 2007]. Figure 15 shows that the composition of Ben's Clod may be consistent with an altered Wishstone or Watchtower class rock.

[67] Taken collectively, these observations indicate that the origin of the Paso Robles class soils is most consistent with condensation from volcanic vapors and precipitation from high-temperature fluids mobilized by volcanic activity in an acid sulfate system. In the terrestrial fumarolic environment, deposits can form as sublimates directly from the gas phase [*Symonds et al.*, 1987]. Liquid condensates, consisting of water with abundant anions and cations can collect and form solid precipitates as the water cools and evaporates [*Stoiber and Rose*, 1970]. A combination of these processes associated with fumarolic emissions are likely responsible for the formation of the Paso Robles class deposits.

[68] This interpretation implies a sulfur-rich magmatic source, which has been previously hypothesized [*Clark and Baird*, 1979], or the presence of nearby iron sulfide deposits. The possible detection of pyrite and/or marcasite in one rock sample on Home Plate [*Morris et al.*, 2007] supports the idea of crustal sulfides. However, this identification is not certain [*Squyres et al.*, 2007], and the continued search for sulfides with the Mössbauer spectrometer is warranted.

8. Biological Implications and Timescales

[69] A sulfurous hydrothermal environment, as indicated by the Paso Robles class soils, can provide the necessary access to water and an energy source to support potential Martian microorganisms. Chemoautotrophic bacteria can utilize H_2, H_2S, and elemental sulfur found in hydrothermal environments in a redox reaction to produce sufficient energy to support metabolic functions [*McKay*, 1997]. This environment was likely highly acidic, as evidenced by the occurrence of ferric sulfates. Acidophilic bacteria on Earth are known to thrive at pH levels of less than 1 [*Nealson*, 1999], although these acidophiles apparently evolved from organisms that initially arose under more neutral pH conditions. Highly acidic conditions may present a significant obstacle to the origin of life [*Knoll et al.*, 2005], and future astrobiological investigations of Mars should be focused on regions with mineral deposits formed from more neutral solutions.

[70] Few observational constraints are available to estimate the duration of hydrothermal activity in the Columbia Hills where the Paso Robles class soils are found. A sustained presence would clearly be more conducive to biological processes than a brief one. The age of the deposits in relation to other geological units (e.g., the Gusev plains or Home Plate) is similarly difficult to constrain. The Columbia Hills may have formed as a result of uplift associated with the formation of ancient craters [*McCoy et al.*, 2008]. These impacts may have resulted in hydrothermal activity [*Newsom et al.*, 1999] similar to the volcanic processes suggested for the development of the Paso Robles class soils. However, it is perhaps significant in terms of their age that these extraordinarily sulfate-rich deposits at Gusev are all found in shallow soil exposures. Soil on Mars undergoes mixing by processes that include redistribution by wind and stirring by impacts. These processes clearly were important at the time of emplacement of the local bedrock, but they have also continued, albeit at lower rates, up to the present. Given the apparently undisturbed nature of the Paso Robles class soils,

it would seem unlikely that they would have remained intact from a time when impact-related hydrothermal processes were relevant. In addition, we cannot rule out the possibility that the local hydrothermal activity that produced Paso Robles class soils took place significantly more recently than major volcanic events in Gusev Crater such as the emplacement of Home Plate and the Adirondack class basalts of the plains. Regardless of the timing, however, the existence of the Paso Robles class soils indicates that transient warm and wet regions consistent with localized habitable environments have been available on Mars.

9. Conclusions

[71] Light-toned soil exposures referred to as Paso Robles class deposits analyzed by the Spirit rover within Gusev crater are hydrated and dominated by ferric sulfates, silica, and magnesium sulfates. Calcium sulfates and phosphates may also be present in certain samples. The presence of ferric sulfates indicates that these soils formed under oxidizing and acidic conditions.

[72] These soils contain the elemental signatures of mobile elements in nearby rocks providing compelling evidence for fluid interactions with these rocks prior to formation of the soil deposits. Compositional differences across the multiple exposures of Paso Robles class soils indicate that these fluids were localized. Significant chemical variability over meter scales is evidence that the quantity of water was limited and that the precipitates did not form under large-scale equilibrium conditions.

[73] Paso Robles class soils are found immediately beneath thin layers of basaltic soil in a variety of topographic settings including within local depressions and on slopes. The formation of this class of soils is therefore not controlled by topography. Minimal contamination from basaltic soil, with the exception of the material mixed in by the rover wheels, indicates that these soils were discovered at or very near the locations where they formed.

[74] The likely formation mechanism for Paso Robles class soils involves hydrothermal fluids and volcanic vapors rich in sulfur, either from magma degassing or perhaps through interactions with crustal sulfide deposits, rising to the surface and producing condensates. The mineral assemblages, chemical signatures, and geologic setting are all consistent with this formation scenario.

[75] Localized warm and wet conditions with sulfur-rich gases provided a potentially habitable environment, although very low pH would have presented a significant environmental challenge to organisms not adapted to such conditions.

[76] **Acknowledgments.** We thank the members of the MER project who enable daily science observations at the Spirit and Opportunity landing sites. We thank K. Herkenhoff for Microscopic Imager images, W. Chen for traverse maps, K. Di for contour plots, and S. McLennan for helpful discussions. J. Bishop and H. Newsom provided constructive reviews of the manuscript. A portion of the work described in this paper was conducted at the Jet Propulsion Laboratory, California Institute of Technology, under a contract with the National Aeronautics and Space Administration.

References

Africano, F., and A. Bernard (2000), Acid alteration in the fumarolic environment of Usu volcano, Hokkaido, Japan, *J. Volcanol. Geotherm. Res.*, *97*, 475–495.

Alexander, G. B., W. M. Heston, and R. K. Iler (1954), The solubility of amorphous silica in water, *J. Phys. Chem.*, *58*, 453–455.

Bell, J. F., III, et al. (2003), Mars Exploration Rover Athena Panoramic Camera (Pancam) investigation, *J. Geophys. Res.*, *108*(E12), 8063, doi:10.1029/2003JE002070.

Bibring, J. P., et al. (2005), Mars surface diversity as revealed by the OMEGA/Mars Express observations, *Science*, *307*, 1576–1581, doi:10.1126/science.1108806.

Bigham, J. M., and D. K. Nordstrom (2000), Iron and aluminum hydroxysulfates from acid sulfate waters, in *Sulfate Minerals: Crystallography, Geochemistry, and Environmental Significance*, *Rev. Mineral.*, vol. 40, edited by C. N. Alpers, J. L. Jambor, and D. K. Nordstrom, pp. 351–403, Mineral. Soc. of Am., Washington, D. C.

Burns, R. G., and S. L. Martinez (1991), Mössbauer spectra of olivine-rich achondrites: Evidence for preterrestrial redox reactions, *Proc. Lunar Planet. Sci.*, *21*, 331–340.

Cabrol, N. A., et al. (2003), Exploring Gusev Crater with Spirit: Review of science objectives and testable hypotheses, *J. Geophys. Res.*, *108*(E12), 8076, doi:10.1029/2002JE002026.

Campbell, J. L., R. Gellert, M. Lee, C. L. Mallet, J. A. Maxwell, and J. M. O'Meara (2008), Quantitative in situ determination of hydration of bright high-sulfate Martian soils, *J. Geophys. Res.*, *113*, E06S11, doi:10.1029/2007JE002959.

Channing, A., and I. B. Butler (2007), Cryogenic opal-A deposition from Yellowstone hot springs, *Earth Planet. Sci. Lett.*, *257*, 121–131.

Christensen, P. R., et al. (2003), Miniature Thermal Emission Spectrometer for the Mars Exploration Rovers, *J. Geophys. Res.*, *108*(E12), 8064, doi:10.1029/2003JE002117.

Christensen, P. R., et al. (2004), Initial results from the Mini-TES experiment in Gusev Crater from the Spirit Rover, *Science*, *305*, 837–842, doi:10.1126/science.1100564.

Clark, B. C., and A. K. Baird (1979), Is the Martian lithosphere sulfur rich?, *J. Geophys. Res.*, *84*, 8395–8403.

Clark, B. C., et al. (2005), Chemistry and mineralogy of outcrops at Meridiani Planum, *Earth Planet. Sci. Lett.*, *240*, 73–94.

Clark, B. C., et al. (2007), Evidence for Montmorillonite or its compositional precursors in Columbia Hills, Mars, *J. Geophys. Res.*, *112*, E06S01, doi:10.1029/2006JE002756.

Crumpler, L. S., T. McCoy, M. Schmidt, and N. Cabrol (2007), Physical volcanology at Gusev Crater, Spirit Rover, in *Seventh International Conference on Mars*, Abstract 3385, Jet Propul. Lab., Pasadena, Calif.

Fournier, R. O., and R. W. Potter II (1982), An equation correlating the solubility of quartz in water from 20° to 900°C at pressures up to 10,000 bars, *Geochim. Cosmochim. Acta*, *46*, 1969–1973.

Gellert, R., et al. (2006), Alpha Particle X-Ray Spectrometer (APXS): Results from Gusev Crater and calibration report, *J. Geophys. Res.*, *111*, E02S05, doi:10.1029/2005JE002555.

Getahun, A., M. H. Reed, and R. Symonds (1996), Mount St. Augustine volcano fumarole wall rock alteration: Mineralogy, zoning, composition and numerical models of its formation process, *J. Volcanol. Geotherm. Res.*, *71*, 73–107.

Glotch, T. D., and J. L. Bandfield (2006), Determination and interpretation of surface and atmospheric Miniature Thermal Emission Spectrometer spectral end-members at the Meridiani Planum landing site, *J. Geophys. Res.*, *111*, E12S06, doi:10.1029/2005JE002671.

Glotch, T. D., J. L. Bandfield, P. R. Christensen, W. M. Calvin, S. M. McLennan, B. C. Clark, A. D. Rogers, and S. W. Squyres (2006), Mineralogy of the light-toned outcrop at Meridiani Planum as seen by the Miniature Thermal Emission Spectrometer and implications for its formation, *J. Geophys. Res.*, *111*, E12S03, doi:10.1029/2005JE002672.

Golombek, M. P., et al. (2003), Selection of the Mars Exploration Rover landing sites, *J. Geophys. Res.*, *108*(E12), 8072, doi:10.1029/2003JE002074.

Griffes, J. L., R. E. Arvidson, F. Poulet, and A. Gendrin (2007), Geologic and spectral mapping of etched terrain deposits in northern Meridiani Planum, *J. Geophys. Res.*, *112*, E08S09, doi:10.1029/2006JE002811.

Herkenhoff, K. E., et al. (2003), Athena Microscopic Imager investigation, *J. Geophys. Res.*, *108*(E12), 8065, doi:10.1029/2003JE002076.

Jambor, J. L., D. K. Nordstrom, and C. N. Alpers (2000), Metal-sulfate salts from sulfide mineral oxidation, in *Sulfate Minerals: Crystallography, Geochemistry, and Environmental Significance*, *Rev. Mineral.*, vol. 40, edited by C. N. Alpers, J. L. Jambor, and D. K. Nordstrom, pp. 303–350, Mineral. Soc. of Am., Washington, D. C.

Joeckel, R. M., B. J. Ang Clement, and L. R. VanFleet Bates (2005), Sulfate-mineral crusts from pyrite weathering and acid rock drainage in the Dakota Formation and Graneros Shale, Jefferson County, Nebraska, *Chem. Geol.*, *215*, 433–452, doi:10.1016/j.chemgeo.2004.06.044.

Johnson, J. R., J. F. Bell III, E. Cloutis, M. Staid, W. H. Farrand, T. McCoy, M. Rice, A. Wang, and A. Yen (2007), Mineralogic constraints on sulfur-rich soils from Pancam spectra at Gusev crater, Mars, *Geophys. Res. Lett.*, *34*, L13202, doi:10.1029/2007GL029894.

Keith, D. C., D. D. Runnells, K. J. Esposito, J. A. Chermak, D. B. Levy, S. R. Hannula, M. Watts, and L. Hall (2001), Geochemical models of the impact of acidic groundwater and evaporative sulfate salts on Boulder Creek at Iron Mountain, California, *Appl. Geochem*, *16*, 947–961.

Keith, T. E. C. (1991), Fossil and active fumaroles in the 1912 eruptive deposits, Valley of Ten Thousand Smokes, Alaska, *J. Volcanol. Geotherm. Res.*, *45*, 227–254.

Klingelhöfer, G., et al. (2003), Athena MIMOS II Mössbauer spectrometer investigation, *J. Geophys. Res.*, *108*(E12), 8067, doi:10.1029/2003JE002138.

Klingelhöfer, G., et al. (2004), Jarosite and hematite at Meridiani Planum from Opportunity's Mössbauer Spectrometer, *Science*, *306*, 1740–1745, doi:10.1126/science.1104653.

Knoll, A. H., et al. (2005), An astrobiological perspective on Meridiani Planum, *Earth Planet. Sci. Lett.*, *240*, 179–189, doi:10.1016/j.epsl.2005.09.045.

Krauskopf, K. B. (1956), Dissolution and precipitation of silica at low temperatures, *Geochim. Cosmochim. Acta*, *10*, 1–26.

Lane, M. D., J. L. Bishop, M. D. Dyar, M. Parente, P. L. King, and B. C. Hyde (2007), The ferric sulfate and ferric phosphate minerals in the light-toned Paso Robles rover track soils: A multi-instrument analysis, in *Seventh International Conference on Mars*, Abstract 3331, Jet Propul. Lab., Pasadena, Calif.

Larsen, K. W., R. E. Arvidson, B. L. Jolliff, and B. C. Clark (2000), Correspondence and least squares analyses of soil and rock compositions for the Viking Lander 1 and Pathfinder landing sites, *J. Geophys. Res.*, *105*, 29,207–29,221.

McCoy, T. J., et al. (2008), Structure, stratigraphy, and origin of Husband Hill, Columbia Hills, Gusev Crater, Mars, *J. Geophys. Res.*, doi:10.1029/2007JE003041, in press.

McKay, C. P. (1997), The search for life on Mars, *Origins Life Evol. Biosphere*, *27*, 263–289.

McLennan, S. M., et al. (2005), Provenance and diagenesis of the evaporite-bearing Burns formation, Meridiani Planum, Mars, *Earth Planet. Sci. Lett.*, *240*, 95–121, doi:10.1016/j.epsl.2005.09.041.

McSween, H. Y., and A. H. Treiman (1998), Martian meteorites, in *Planetary Materials*, *Rev. Mineral.*, vol. 36, edited by J. J. Papike, pp. 6-1 to 6-53, Mineral. Soc. of Am., Washington, D. C.

Ming, D. W., et al. (2006), Geochemical and mineralogical indicators for aqueous processes in the Columbia Hills of Gusev crater, Mars, *J. Geophys. Res.*, *111*, E02S12, doi:10.1029/2005JE002560.

Mittlefehldt, D. W., R. Gellert, T. McCoy, H. Y. McSween Jr., R. Li, and the Athena Science Team (2006), Possible Ni-rich mafic-ultramafic magmatic sequence in the Columbia Hills: Evidence from the Spirit rover, *Lunar Planet. Sci.*, *XXXVII*, 1505.

Morris, R. V., et al. (2000), Acid sulfate alteration products of a tholeiitic basalt: Implications for interpretation of Martian thermal emission spectra, *Lunar Planet. Sci. Conf.*, *XXXI*, 2014.

Morris, R. V., et al. (2004), Mineralogy at Gusev Crater from the Mössbauer spectrometer on the Spirit Rover, *Science*, *305*, 833–836, doi:10.1126/science.1100020.

Morris, R. V., et al. (2006), Mössbauer mineralogy of rock, soil, and dust at Gusev crater, Mars: Spirit's journey through weakly altered olivine basalt on the plains and pervasively altered basalt in the Columbia Hills, *J. Geophys. Res.*, *111*, E02S13, doi:10.1029/2005JE002584.

Morris, R. V., et al. (2007), Possible evidence for iron sulfate, iron sulfides, and elemental sulfur at Gusev Crater, Mars, from MER, CRISM, and analog data, in *Seventh International Conference on Mars*, Abstract 3393, Jet Propul. Lab., Pasadena, Calif.

Nealson, K. H. (1999), Post-Viking microbiology: New approaches, new data, new insights, *Origins Life Evol. Biosphere*, *29*, 73–93.

Newsom, H. E., J. J. Hagerty, and F. Goff (1999), Mixed hydrothermal fluids and the origin of the Martian soil, *J. Geophys. Res.*, *104*, 8717–8728.

Nomura, K., M. Takeda, T. Iiyama, and H. Sakai (2005), Mössbauer studies of jarosite, mikasaite and yavapaiite, and implication to their Martian counterparts, *Hyperfine Interact.*, *166*, 657–664, doi:10.1007/s10751-006-9337-y.

Nordstrom, D. K., and C. N. Alpers (1999), Negative pH, efflorescent mineralogy, and consequences for environmental restoration at the Iron Mountain Superfund site, California, *Proc. Natl. Acad. Sci. U. S. A.*, *96*, 3455–3462.

Ohba, T., and M. Nakagawa (2002), Minerals in volcanic ash 2: Non-magmatic minerals, *Global Environ. Res.*, *6*, 53–59.

Rieder, R., R. Gellert, J. Brückner, G. Klingelhöfer, G. Dreibus, A. Yen, and S. W. Squyres (2003), The new Athena alpha particle X-ray spectrometer for the Mars Exploration Rovers, *J. Geophys. Res.*, *108*(E12), 8066, doi:10.1029/2003JE002150.

Squyres, S. W., et al. (2006), Rocks of the Columbia Hills, *J. Geophys. Res.*, *111*, E02S11, doi:10.1029/2005JE002562.

Squyres, S. W., et al. (2007), Pyroclastic activity at Home Plate in Gusev Crater, Mars, *Science*, *316*, 738–742, doi:10.1126/science.1139045.

Stoiber, R. E., and W. I. Rose (1970), The geochemistry of Central American volcanic gas condensates, *Geol. Soc. Am. Bull.*, *81*, 2891–2912.

Stoiber, R. E., and W. I. Rose (1974), Fumarole incrustations at active Central American volcanoes, *Geochim. Cosmochim. Acta*, *38*, 495–516.

Symonds, R. B., W. I. Rose, M. H. Reed, F. E. Lichte, and D. L. Finnegan (1987), Volatilization, transport and sublimation of metallic and non-metallic elements in high temperature gases at Merapi Volcano, Indonesia, *Geochim. Cosmochim. Acta*, *51*, 2083–2101.

Tosca, N. J., and S. M. McLennan (2007), An experimental approach to evaporation processes at the Martian surface, *Lunar Planet. Sci.*, *XXXVIII*, Abstract 1893.

Wang, A., et al. (2007), Sulfate-rich soils exposed by Spirit rover at multiple locations in Gusev Crater on Mars, in *Seventh International Conference on Mars*, Abstract 3348, Jet Propul. Lab., Pasadena, Calif.

White, D. E., W. W. Brannock, and K. J. Murata (1956), Silica in hot-spring waters, *Geochim. Cosmochim. Acta.*, *10*, 27–59.

Yen, A. S. (2006), Martian sulfates as observed by the Mars Exploration Rover Mössbauer and alpha particle X-ray spectrometers, *Eos Trans. AGU*, *87*(52), Fall Meet. Suppl., Abstract P22A-02.

Yen, A. S., et al. (2005), An integrated view of the chemistry and mineralogy of Martian soils, *Nature*, *436*, 49–54, doi:10.1038/nature03637.

Zimbelman, D. R., R. O. Rye, and G. N. Breit (2005), Origin of secondary sulfate minerals on active andesitic stratovolcanoes, *Chem. Geol.*, *215*, 37–60, doi:10.1016/j.chemgeo.2004.06.056.

R. Arvidson, Department of Earth and Planetary Sciences, Washington University Campus Box 1169, One Brookings Drive, St. Louis, MO 63130, USA.

B. C. Clark, Lockheed Martin Corporation, MS S8000, P.O. Box 179, 12257 State Highway 121, Littleton, CO 80127, USA.

R. Gellert, Department of Physics, University of Guelph, Guelph, ON, Canada N1G 2W1.

J. Hurowitz and A. S. Yen, Jet Propulsion Laboratory, Mail Stop 183-501, 4800 Oak Grove Drive, Pasadena, CA 91109, USA.

J. R. Johnson, U.S. Geological Survey, Astrogeology Team, 2255 N. Gemini Drive, Flagstaff, AZ 86001, USA.

A. T. Knudson, Department of Earth and Planetary Sciences, Arizona State University, Mail Code 6305, Tempe, AZ 85287, USA.

R. Li, CEEGS/Center for Mapping, Ohio State University, 470 Hitchcock Hall, 2070 Neil Avenue, Columbus, OH 43210, USA.

T. McCoy and M. Schmidt, Department of Mineral Sciences, National Museum of Natural History, Smithsonian Institution, 10th and Constitution Avenues, N.W., Washington, DC 20560, USA.

D. W. Ming, NASA Johnson Space Center, Code KX, 2101 NASA Parkway, Houston, TX 77058, USA.

D. W. Mittlefehldt and R. V. Morris, NASA Johnson Space Center, Code KR, 2101 NASA Parkway, Houston, TX 77058, USA.

S. Squyres, Department of Astronomy, Cornell University, 428 Space Sciences, Ithaca, NY 14853, USA.